Protein phosphatase 4 catalytic subunit regulates Cdk1 activity and microtubule organization via NDEL1 dephosphorylation

Kazuhito Toyo-oka,[1] Daisuke Mori,[1] Yoshihisa Yano,[1] Masayuki Shiota,[2] Hiroshi Iwao,[2] Hidemasa Goto,[3] Masaki Inagaki,[3] Noriko Hiraiwa,[4] Masami Muramatsu,[5] Anthony Wynshaw-Boris,[6,7] Atsushi Yoshiki,[4] and Shinji Hirotsune[1]

[1]Department of Genetic Disease Research and [2]Department of Pharmacology, Osaka City University Graduate School of Medicine, Osaka 545-8586, Japan
[3]Division of Biochemistry, Aichi Cancer Center Research Institute, Aichi 464-8681, Japan
[4]Experimental Animal Division, Department of Biological Systems, BioResource Center, RIKEN Tsukuba Institute, Ibaraki 305-0074, Japan
[5]Division of Neuroscience, Research Center for Genomic Medicine, Saitama Medical School, Saitama 350-1241, Japan
[6]Department of Pediatrics and [7]Institute of Human Genetics, School of Medicine, University of California, San Fransisco, San Francisco, CA 94143

Protein phosphatase 4 catalytic subunit (PP4c) is a PP2A-related protein serine/threonine phosphatase with important functions in a variety of cellular processes, including microtubule (MT) growth/organization, apoptosis, and tumor necrosis factor signaling. In this study, we report that NDEL1 is a substrate of PP4c, and PP4c selectively dephosphorylates NDEL1 at Cdk1 sites. We also demonstrate that PP4c negatively regulates Cdk1 activity at the centrosome. Targeted disruption of *PP4c* reveals disorganization of MTs and disorganized MT array. Loss of PP4c leads to an unscheduled activation of Cdk1 in interphase, which results in the abnormal phosphorylation of NDEL1. In addition, abnormal NDEL1 phosphorylation facilitates excessive recruitment of katanin p60 to the centrosome, suggesting that MT defects may be attributed to katanin p60 in excess. Inhibition of Cdk1, NDEL1, or katanin p60 rescues the defective MT organization caused by PP4 inhibition. Our work uncovers a unique regulatory mechanism of MT organization by PP4c through its targets Cdk1 and NDEL1 via regulation of katanin p60 distribution.

Introduction

The vertebrate centrosome is a highly organized organelle that serves as the cell microtubule (MT) organizing center, among other functions (Doxsey, 2001; Bornens, 2002). During interphase, MTs are organized in astral arrays that radiate from the centrosome and function as a scaffold to direct organelle and vesicle trafficking (Thyberg and Moskalewski, 1999). One particular dramatic change is loss of the extensive interphase MT array and the subsequent assembly of a bipolar mitotic spindle (Compton, 2000). Progress in understanding how centrosomal MT arrays are regulated has revealed that many proteins participate in the nucleation (γ-tubulin and pericentrin), anchoring (ninein, centriolin, dynactin, XMAP215, and TACCs), and release (katanin and XKCM1/mitotic centromere-associated kinesin) of MTs from the centrosome (Walczak et al., 1996; Doxsey, 2001; Bornens, 2002; Kinoshita et al., 2002; Blagden and Glover, 2003). MTs and these accessory components are also critically regulated by mitotic kinases, including Cdk1, the Polo family, the NIMA (never in mitosis A) family, and the Aurora family, upon entrance into mitosis (Nigg, 2001; Blagden and Glover, 2003). Whereas protein kinases regulate protein activities by phosphorylating key residues on the molecules, protein phosphatases counteract kinase activities by dephosphorylating those residues. Protein phosphatases, including Cdc14A, Cdc25C, PP1, and PP4, have been shown to associate with mitotic centrosomes (Ou and Rattner, 2004). Both PP1 and PP4 are members of the PPP family of protein serine/threonine phosphatases, which associate with the centrosome during mitosis (Brewis et al., 1993; Andreassen et al., 1998; Helps et al., 1998). The orchestrated modulation of centrosomal components by kinases and phosphatases plays an essential role for the maintenance of MT organization and spindle formation (Meraldi and Nigg, 2001).

Accumulating evidence suggests that centrosomal components and their kinases play critical roles in neurogenesis and neuronal migration (Wynshaw-Boris and Gambello, 2001; Tsai and Gleeson, 2005). *LIS1* was identified as a gene mutated in

K. Toyo-oka and D. Mori equally contributed to this paper.

Correspondence to Shinji Hirotsune: shinjih@med.osaka-cu.ac.jp

Abbreviations used in this paper: KLH, keyhole limpet hemocyanin; MEF, mouse embryonic fibroblast; MT, microtubule; PP4c, protein phosphatase 4 catalytic subunit.

The online version of this article contains supplemental material.

The Journal of Cell Biology, Vol. 180, No. 6, March 24, 2008 1133–1147
http://www.jcb.org/cgi/doi/10.1083/jcb.200705148

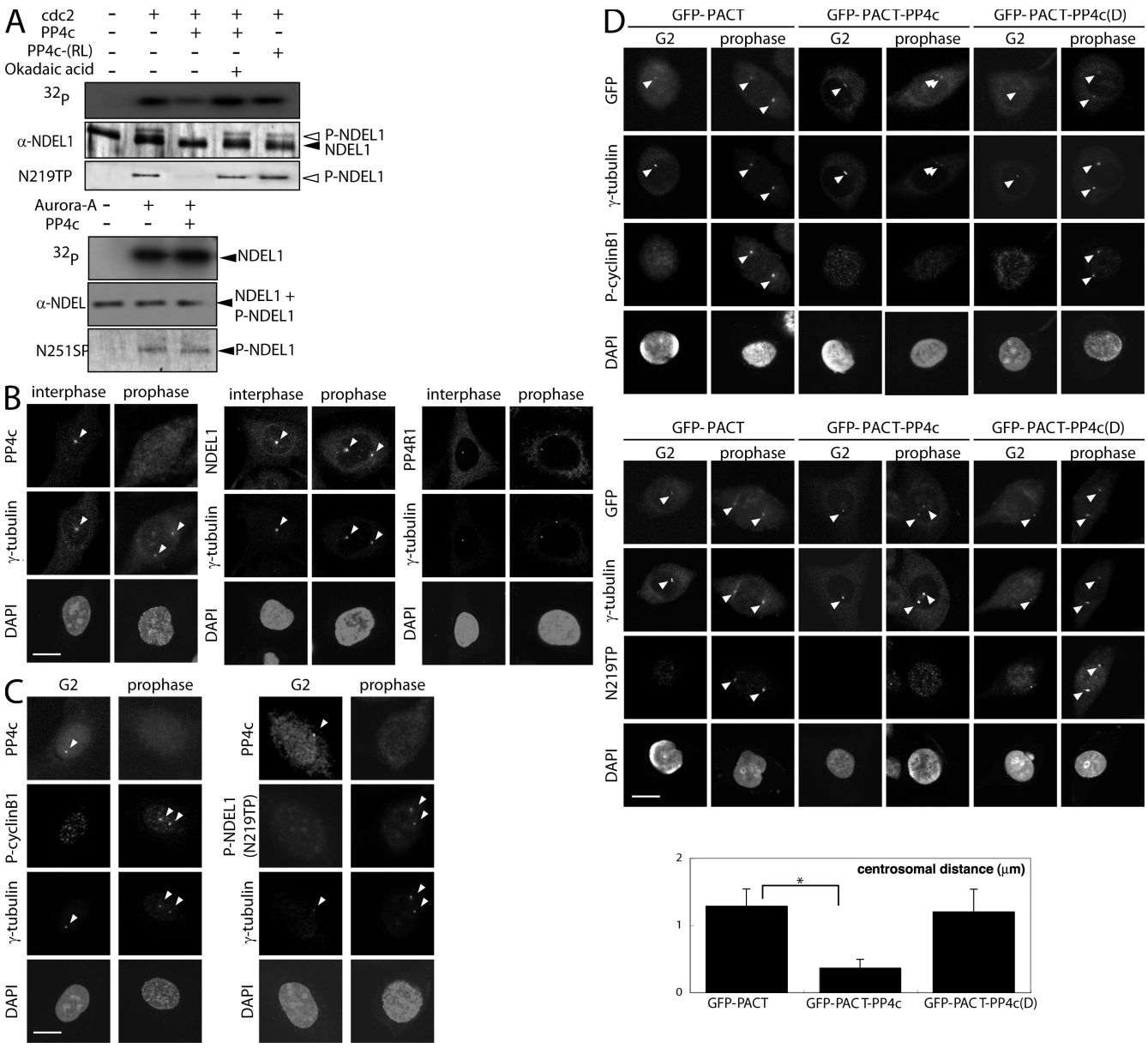

Figure 1. **PP4c dephosphorylates NDEL1 at Cdk1 sites and suppresses Cdk1 activation.** (A, top) We examined whether PP4c dephosphorylates phospho-NDEL1 (P-NDEL1) that was phosphorylated by GST-Cdk1 using recombinant proteins. Note the lower mobility of NDEL1 phosphorylated by GST-Cdk1. PP4c efficiently removed phosphate from one of the Cdk1 phosphorylation sites of NDEL1 (T219). (bottom) We tested whether GST-PP4c dephosphorylates P-NDEL1 phosphorylated by Aurora A kinase. GST-PP4c did not show any dephosphorylation activity at the GST–Aurora A phosphorylation site (S251). Western blotting pattern using an anti-NDEL1, an antiphospho-T219 antibody (Cdk1 site), or an antiphospho-S251 antibody (Aurora A site) is shown at the bottom of each. Note that signal by antiphospho-T219 antibody was diminished after dephosphorylation by PP4c. (B) Subcellular distribution of PP4c (left), NDEL1 (middle), and PP4R1 (right) in asynchronously growing HeLa cells at interphase or prophase (representative images of three independent experiments). Arrowheads indicate centrosomes. (C) Examination of PP4c distribution and phosphorylation of cyclin B1 (left) and NDEL1 (right). Synchronously growing HeLa cells were stained with the indicated antibodies for phosphorylated proteins. Arrowheads indicate the centrosomes (representative images of three independent experiments). (D) Persistent expression of PP4c at the centrosome prevented phosphorylation of cyclin B1 (top) and NDEL1 (middle). Synchronously growing HeLa cells transfected with constructs as indicated above the panels were costained with the indicated antibodies. Images were captured at G2 or prophase. The distances of separated centrosomes are summarized at the bottom (representative images of five independent experiments). (bottom) Statistical analysis of centrosomal distances. The p-value was calculated using an unpaired *t* test (*, $P < 0.001$; one example of three independent experiments; $n = 200$). Error bars represent SEM. Bars, 10 μm.

isolated lissencephaly sequence (Reiner et al., 1993), which is a cerebral cortical malformation characterized by a smooth cerebral surface and a disorganized cortex caused by incomplete neuronal migration (Dobyns, 1989; Dobyns et al., 1993). LIS1 and its binding partner, NDEL1, are preferentially distributed at the centrosome (Sasaki et al., 2000) and regulate the cytoplasmic dynein heavy chain (Vallee, 1991; Vallee et al., 2001). *Lis1*- and *Ndel1*-disrupted mice displayed similar defects in neuronal migration (Hirotsune et al., 1998; Sasaki et al., 2005). Interestingly, NDEL1 is a known substrate of several kinases, including

Cdk5/Cdk1, which are essential for regulation of a proper MT organization (Toyo-Oka et al., 2005). In addition, Cdk5/Cdk1-mediated phosphorylation of NDEL1 recruits katanin p60, which controls MT dynamics (McNally and Vale, 1993; McNally, 2000) at the centrosome and facilitates MT remodeling (Toyo-Oka et al., 2005). Recently, we also demonstrated that NDEL1 is phosphorylated by Aurora A kinase, which is essential for centrosomal maturation and separation (Mori et al., 2007). These observations led us to clarify the precise functions of NDEL1 in MT dynamics.

In this study, we report that NDEL1 is a substrate of the centrosomal phosphatase protein phosphatase 4 catalytic subunit (PP4c; Helps et al., 1998; Hu et al., 1998). PP4c efficiently dephosphorylates Cdk1 sites of NDEL1 but does not dephosphorylate the Aurora A site. We also found that PP4c negatively regulates Cdk1 activity in interphase. To understand the physiological role of PP4c in vivo, we generated *PP4c*-disrupted mice by Cre-loxP recombination. Mouse embryonic fibroblast (MEF) cells in which *PP4c* was deleted by Cre exhibited severe impairments of MT organization. Surprisingly, loss of PP4c led to an unscheduled activation of Cdk1 at interphase and an up-regulation of the T219 phosphorylation of NDEL1 in interphase, which is associated with an excessive accumulation of katanin p60 to the centrosome. These findings suggest that PP4c is required for proper organization of MTs at the centrosome through regulation of the phosphorylation of NDEL1 and recruitment of katanin p60.

Results

PP4c specifically dephosphorylates NDEL1 at phosphorylation sites of Cdk5/Cdk1 and regulates the activity of Cdk1

To identify proteins interacting with NDEL1, we performed a yeast two-hybrid analysis using NDEL1 as bait and identified PP4c (Helps et al., 1998; Hu et al., 1998). We next examined the ability of PP4c to dephosphorylate a Cdk1 phosphorylation site, phospho-T219 (Toyo-Oka et al., 2005), and an Aurora A phosphorylation site, phospho-S251 (Mori et al., 2007), of NDEL1 using recombinant proteins as a substrate. NDEL1 was initially subjected to phosphorylation by GST-Cdk1 or GST–Aurora A (Mori et al., 2007), and phosphoproteins were purified before the dephosphorylation experiments. PP4c efficiently removed the phosphate from Cdk1 phosphorylation sites but not from the Aurora A phosphorylation site (Fig. 1 A). The dephosphorylation activity of PP4c was completely suppressed by okadaic acid. In addition, the PP4c inactive mutant, PP4c-RL, in which Arg236 was replaced with Leu (Zhou et al., 2002), did not display any dephosphorylation activity (Fig. 1 A). We also confirmed dephosphorylation by PP4c by Western blotting. PP4c treatment selectively diminished the signal of Western blotting by an antiphospho-T219 antibody (Fig. 1 A). These results suggested that at least one of the Cdk1 phosphorylation sites of NDEL1 is a specific substrate of PP4c.

We next tested the subcellular distribution of NDEL1, PP4c, and another binding protein of PP4c, R1 (Kloeker and Wadzinski, 1999). In interphase, PP4c was predominantly distributed at the centrosome and inside the nucleus, whereas the signal of PP4c disappeared from the centrosome during mitosis (Fig. 1 B). In contrast to the cell cycle–dependent distribution of PP4c, NDEL1 and R1 were stably localized at the centrosome regardless of the cell cycle (Fig. 1 B). Western blotting on synchronized HeLa cells indicated that PP4c protein levels were equivalent throughout the cell cycle (unpublished data). We next sought to characterize whether the presence of PP4c is related to the phosphorylation of cyclin B1 and NDEL1. We examined S126 phosphorylation of human cyclin B1, the site of the mitosis-specific phosphorylation of cyclin B1 by activated Cdk1 (Jackman et al., 2003) and T219 phosphorylation of NDEL1 (Toyo-Oka et al., 2005). Although immunocytochemistry showed virtually no phosphorylation of human cyclin B1 and T219 of NDEL1 in interphase, robust phosphorylation was seen after the mitotic entry. Conversely, PP4c localized to the centrosome in interphase but disappeared from the centrosome after mitotic entry (Fig. 1 C). These findings suggest that that PP4c normally may prevent activation of Cdk1 at the centrosome.

We next asked whether the persistent expression of PP4c might inhibit the activation of Cdk1. To achieve restricted expression of PP4c at the centrosome, we conjugated PP4c to a PACT domain (Gillingham and Munro, 2000). Prolonged centrosomal expression of PACT-PP4c clearly abolished cyclin B1 S126 phosphorylation and suppressed the separation of centrosomes in prophase (Fig. 1 D), whereas activation of Aurora A was still observed by monitoring T288 phosphorylation (not depicted). In contrast, the expression of a control PACT domain or PACT-PP4c-RL did not display this effect (Fig. 1 D). Phosphorylation of NDEL1 was also clearly suppressed by the centrosomal expression of PP4c (Fig. 1 D).

To examine the dephosphorylation activity of NDEL1 by PP4c in vivo, we coexpressed *PACT-PP4c* and *PACT–mitotic Cdk1* (Litvak et al., 2004) and examined the phosphorylation of NDEL1 and human cyclin B1 in G2. The expression of PACT–mitotic Cdk1 led to the phosphorylation of cyclin B1 and NDEL1 (Fig. 2 A), whereas the coexpression of PACT–mitotic cyclin and PACT-PP4c clearly suppressed the phosphorylation of both proteins, suggesting that PP4c is capable of dephosphorylating cyclin B1 and NDEL1 in vivo and that PP4c might be functionally dominant over Cdk1. We previously reported that phosphorylation of NDEL1 by Cdk1 facilitates recruitment of katanin p60 at the centrosome (Toyo-Oka et al., 2005). Therefore, we examined whether the expression of mitotic Cdk1 in G2 facilitates the recruitment of katanin p60 at the centrosome. Interestingly, the expression of PACT–mitotic Cdk1 in G2 HeLa cells increased the centrosomal localization of katanin p60 and resulted in fewer MTs (Fig. 2 B and see Fig. 5 B).

Loss of PP4c causes MT disorganization

To explore the in vivo role of *PP4c* and its function in the organization of MTs, we generated a mutant line, $PP4c^{neo/+}$ (Fig. S1, A–C; available at http://www.jcb.org/cgi/content/full/jcb.200705148/DC1; and see Materials and methods). We further generated $PP4c^{cko/+}$ and $PP4c^{-/+}$ by a Cre-mediated partial and complete recombination of $PP4c^{neo/+}$ mice, respectively (Fig. S1, A–C; and see Materials and methods). These three lines of heterozygous mutant mice were viable and fertile.

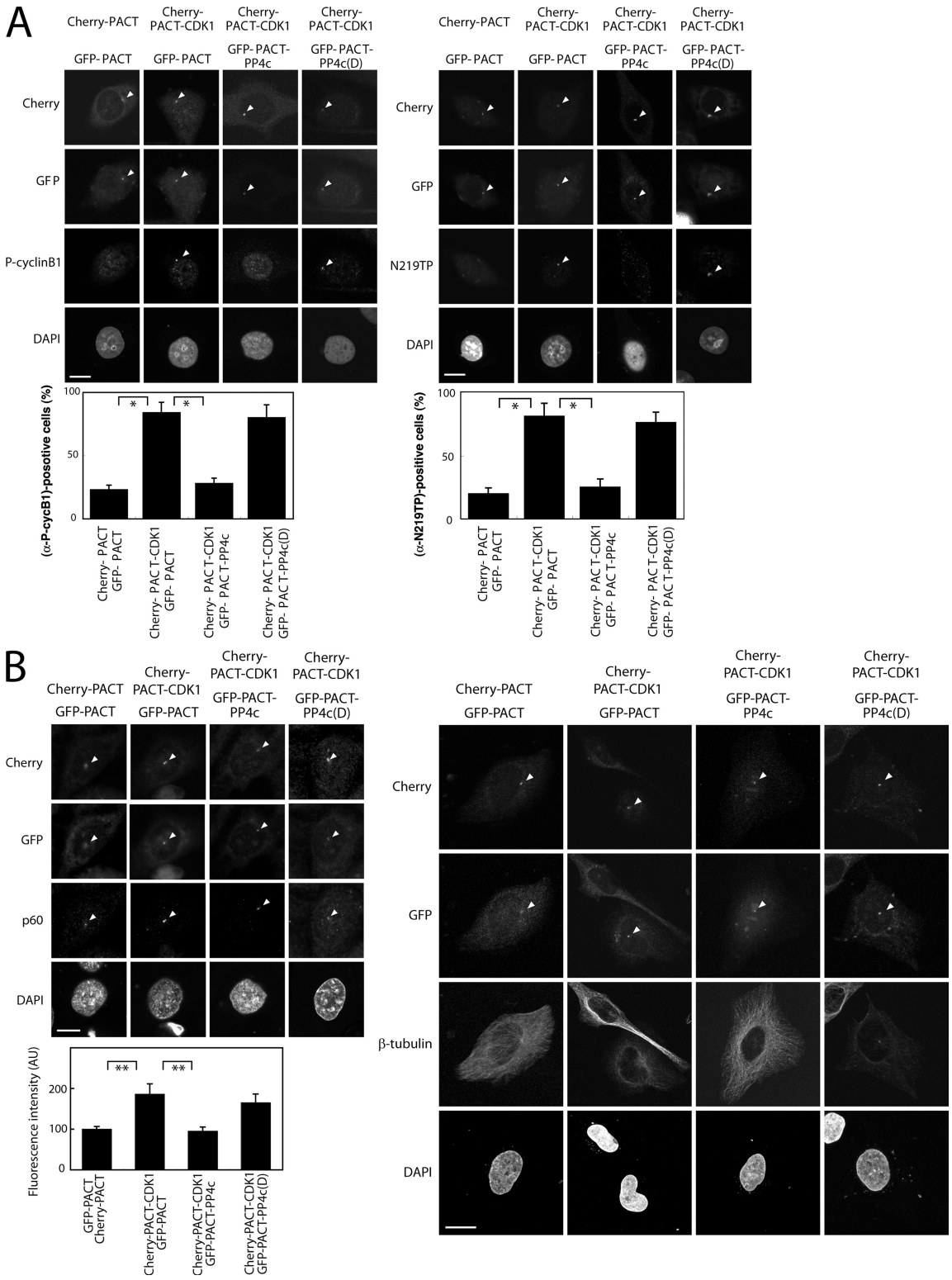

Figure 2. **Functional relationships between PP4c and Cdk1.** (A) PP4c dephosphorylates cyclin B1 (top left) and NDEL1 (top right) in vivo. Synchronously growing HeLa cells cotransfected with constructs as indicated above the panels and were costained with the indicated antibodies. Images were captured at G2. To express active Cdk1 in G2, mitotic Cdk1 was used. Mitotic Cdk1 efficiently phosphorylated cyclin B1 and NDEL1 in vivo in G2. These phosphorylations were clearly abolished by the cotransfection of PP4c. The frequency of phosphorylation is summarized at the bottom (one example of three independent experiments; $n = 100$), and statistical analysis of phosphorylation-positive cells is shown. (B) Expression of mitotic Cdk1 facilitates recruitment of katanin p60 to the centrosome (top left). Synchronously growing HeLa cells were cotransfected with constructs as indicated above the panels and were costained with the indicated antibodies. Images were captured at G2. Expression of mitotic Cdk1 in G2 HeLa cells revealed augmentation of the concentration of katanin p60 at the centrosome (one example of three independent experiments; $n = 100$). The MT array appeared sparsely distributed in mitotic Cdk1-expressed HeLa cells (right). Statistical analysis of the fluorescence intensity of p60 is shown at the bottom left. Error bars represent SEM. (A and B) Arrowheads indicate centrosomes. *, $P < 0.001$; **, $P < 0.05$. Bars, 10 μm.

We generated homozygous mice by the mating of each heterozygote and found that *PP4c*$^{cko/cko}$ mice were viable and fertile, whereas *PP4c*$^{neo/neo}$ mice and *PP4c*$^{-/-}$ mice died in the mid and early embryonic stages, respectively. This is consistent with a previous study (Fig. S1, D–F; Shui et al., 2007).

To analyze the role of PP4c in MT regulation and cell proliferation, we established an MEF line. *PP4c* was inactivated by RFP-Cre–mediated recombination through transfection of a plasmid or adenovirus-mediated gene transfer carrying RFP-Cre (see each figure legend). Cre-mediated recombination efficiently removed part of the *PP4c* gene (*PP4c*$^{-/-}$ MEF cells), resulting in the disruption of *PP4c* (Fig. 3 A). Disruption of *PP4c* in MEF cells resulted in the serious disorganization of MTs (Fig. 3 B), whereas the expression of RFP-Cre in *PP4c*$^{+/+}$ MEF cells did not display any obvious effect on the organization of MTs. We categorized the MT patterns into four groups: normal, in which MTs appeared normal with fiberlike staining and centrosomal focusing; type A, in which MTs were abundant but no obvious centrosomal focusing of the MTs was observed; type B, in which overall MT levels were reduced and remaining MTs appeared to be bundled; and type C, in which only weak diffuse staining and a few fragmented MTs were observed within the cytoplasm. Type C cells were more numerous in cells transfected for longer times (Fig. 3 B). Interestingly, in these cells with profoundly defective MT arrays, the signal of γ-tubulin was comparable with wild type (Fig. 3 A). These observations prompted us to investigate the stability of MTs using an antiacetylated α-tubulin antibody to visualize a stable tubulin (Fig. 3 C). The intensity of antiacetylated tubulin antibody staining was clearly decreased in *PP4c*$^{-/-}$ MEF cells compared with *PP4c*$^{+/+}$ MEF cells, suggesting that MTs became unstable in *PP4c*$^{-/-}$ MEF cells.

In the mouse genome, *PP4c* is located on chromosome 7 adjacent to *Tbx6* (Chapman and Papaioannou, 1998). Inadvertently, the *PGK-neo* gene bracketed by loxP was inserted into the last exon of *Tbx6*, and the last four amino acids were replaced by 15–32 different amino acids, which may influence the function of *Tbx6* (Fig. S2, A and B; available at http://www.jcb.org/cgi/content/full/jcb.200705148/DC1). To exclude the possibility that MT defects might be attributed to impairment of the *Tbx6* gene, we established MEF cells from a *Tbx6*$^{-/-}$ embryo and found normal MT organization (Fig. S2 C). We also confirmed that the impaired organization of MTs was rescued by the exogenous expression of *PP4c* but not by the exogenous expression of *Tbx6* (Fig. S2, D and E). Thus, we concluded that impairment of MT organization is attributable to the loss of *PP4c* rather than the mutation of *Tbx6*.

We previously reported that NDEL1 phosphorylation by Cdk1 recruits katanin p60 to the centrosome (Toyo-Oka et al., 2005). We hypothesized that the defect of MT organization in *PP4c*$^{-/-}$ MEF cells might be attributed to excessive recruitment of katanin p60 to the centrosome, which is associated with the abnormal phosphorylation of NDEL1. To address this possibility, we first examined the phosphorylation of endogenous NDEL1 using known antiphospho-NDEL1 antibodies (Toyo-Oka et al., 2005; Mori et al., 2007). Interestingly, *PP4c*$^{-/-}$ MEF cells displayed abnormal phosphorylation of NDEL1 at the T219 Cdk1 site (Fig. 4 A), whereas S251, the Aurora A site, was not phosphorylated (not depicted). Therefore, we sought to determine whether Cdk1 activity was increased in *PP4c*$^{-/-}$ MEF cells. We raised an antibody against phospho-S123 of mouse cyclin B1, which corresponds to S126 of human cyclin B (Jackman et al., 2003), as an indicator of activated Cdk1 (Fig. S3, available at http://www.jcb.org/cgi/content/full/jcb.200705148/DC1). Surprisingly, Cdk1 was frequently activated in *PP4c*$^{-/-}$ MEF cells as determined by monitoring the mitotic phosphorylation of S123, whereas none of these phosphorylations were observed in interphase of control cells (Fig. 4 B). The activation of Cdk1 in *PP4c*$^{-/-}$ MEF cells was also supported by the enzymatic activity of Cdk1 (Fig. 4 C). GFP-PACT-Cdk1 extracted from *PP4c*$^{-/-}$ MEF cells revealed higher phosphorylation activity compared with control MEF cells, suggesting that Cdk1 is activated in *PP4c*$^{-/-}$ MEF cells. Collectively, our data support the notion that PP4c is a negative regulator of Cdk1.

Phospho-S123 cyclin B1–positive cells in *PP4c*$^{-/-}$ MEF cells rarely displayed chromosome condensation. Although the activation of Cdk1 could occur in interphase, mitotic arrest by activation of the G2/M checkpoint instead of the unscheduled activation of Cdk1 is another possibility. To address this issue, we first examined the cell cycle pattern of *PP4c*$^{-/-}$ MEF cells by flow cytometry. A higher 4c population appeared in *PP4c*$^{-/-}$ MEF cells, suggesting that *PP4c*$^{-/-}$ MEF cells were arrested in G2/M (Fig. 4 D). We next asked whether histone H3, a marker of prophase, was phosphorylated in *PP4c*$^{-/-}$ MEF cells (Fig. 4 D). In *PP4c*$^{-/-}$ MEF cells, phosphorylation of histone H3 was not observed, indicating that *PP4c*$^{-/-}$ MEF cells did not enter into prophase. Furthermore, activation of Cdk1 in *PP4c*$^{-/-}$ MEF cells was observed in MEF cells in which cell cycle was arrested by mitomycin C treatment (Fig. S4, A–C; available at http://www.jcb.org/cgi/content/full/jcb.200705148/DC1) or contact inhibition and serum starvation (Fig. S4 D). Thus, we conclude that Cdk1 is abnormally activated at interphase in *PP4c*$^{-/-}$ MEF cells.

The aberrant MT organization in *PP4c*$^{-/-}$ MEF cells is reminiscent of the disruption of MTs caused by the overexpression of katanin p60 (Fig. 5 A). Therefore, we investigated whether katanin p60 was excessively recruited to the centrosome. Immunostaining revealed that higher amounts of katanin p60 were accumulated at the centrosome in *PP4c*$^{-/-}$ MEF cells (Fig. 5 B). Quantitative analysis of the fluorescence intensity demonstrated a twofold increase of katanin p60 at the centrosome in *PP4c*$^{-/-}$ MEF cells compared with *PP4c*$^{cko/cko}$ MEF cells (Fig. 5 B). As an independent approach to confirm the phosphorylation of NDEL1 and restricted distribution of katanin p60 with centrosomes, we isolated centrosomes from MEF cells and fractionated the protein lysate. Immunoblot analysis of fractions from *PP4c*$^{-/-}$ MEF cells revealed that phosphorylated NDEL1 was indeed present with γ-tubulin, which was cofractionated with katanin p60 (Fig. 5 C; Moudjou and Bornens, 1998). The total amount of katanin p60 was not changed in *PP4c*$^{-/-}$ MEF cells; however, katanin p60 displayed a more restricted distribution compared with *PP4c*$^{cko/cko}$ MEF cells. Our finding suggests that PP4c regulates the organization of MTs partly through regulation of the phosphorylation of NDEL1 and the distribution of katanin p60.

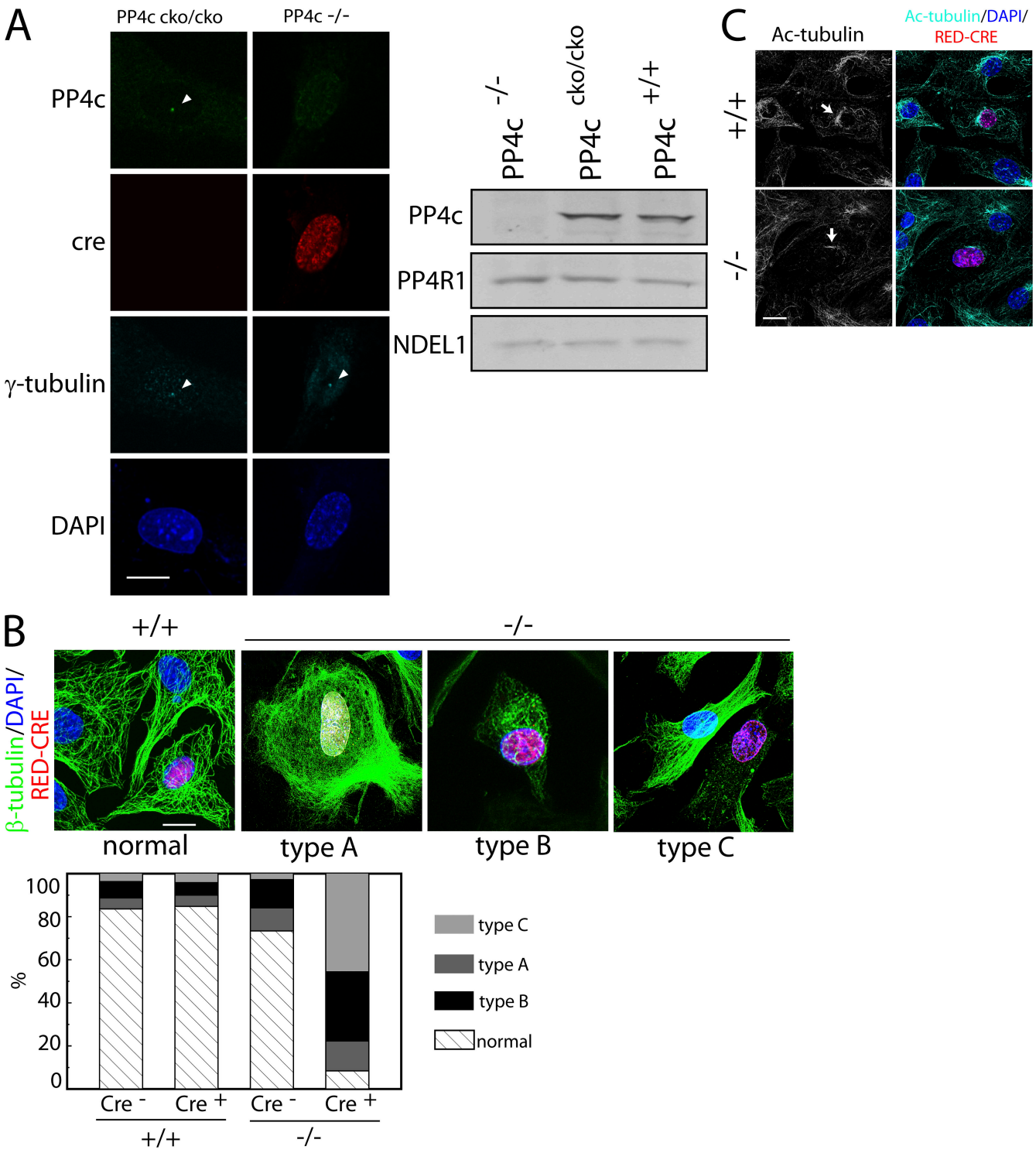

Figure 3. **Disorganization of MTs in *PP4c*$^{-/-}$ MEF cells.** (A) Expression of PP4c in *PP4c*$^{cko/cko}$ and *PP4c*$^{-/-}$ MEF cells. (left) Immunofluorescent staining was performed with an anti-PP4c antibody to assess the expression of PP4c 48 h after infection of *adeno-Cre* (representative of each genotype; *n* = 50). Uninfected *PP4c*$^{cko/cko}$ MEF cells were used as controls. Arrowheads indicate centrosomal staining of PP4c. (right) Western blotting analysis of PP4c, PP4R1, and NDEL1 expression in *PP4c*$^{+/+}$, *PP4c*$^{cko/cko}$, and *PP4c*$^{-/-}$ MEF cells. Representatives of three independent experiments are shown. (B) Severe MT disorganization in *PP4c*$^{-/-}$ MEF cells. MEF cells for each genotype were stained with an anti–β-tubulin antibody 48 h after infection of *adeno-Cre* to *PP4c*$^{cko/cko}$ MEF cells. *PP4c*$^{+/+}$ MEF cells infected with *adeno-Cre* were used for controls. MT patterns were categorized into four groups as indicated at the bottom of each panel. The relative proportions of each pattern are shown in the bottom panel (one example of three independent experiments; *n* = 100 for each genotype). (C) MTs in *PP4c*$^{-/-}$ MEF cells were destabilized. Immunostaining was performed using antiacetylated tubulin 48 h after infection of *PP4c*$^{cko/cko}$ MEF cells with *adeno-Cre*. *PP4c*$^{+/+}$ MEF cells infected with *adeno-Cre* were used for controls. MEF cells lacking PP4c revealed a clear reduction of acetylated tubulin (one example of three independent experiments; *n* = 60 for each genotype). Arrows indicate Cre-positive MEF cells. Bars, 10 μm.

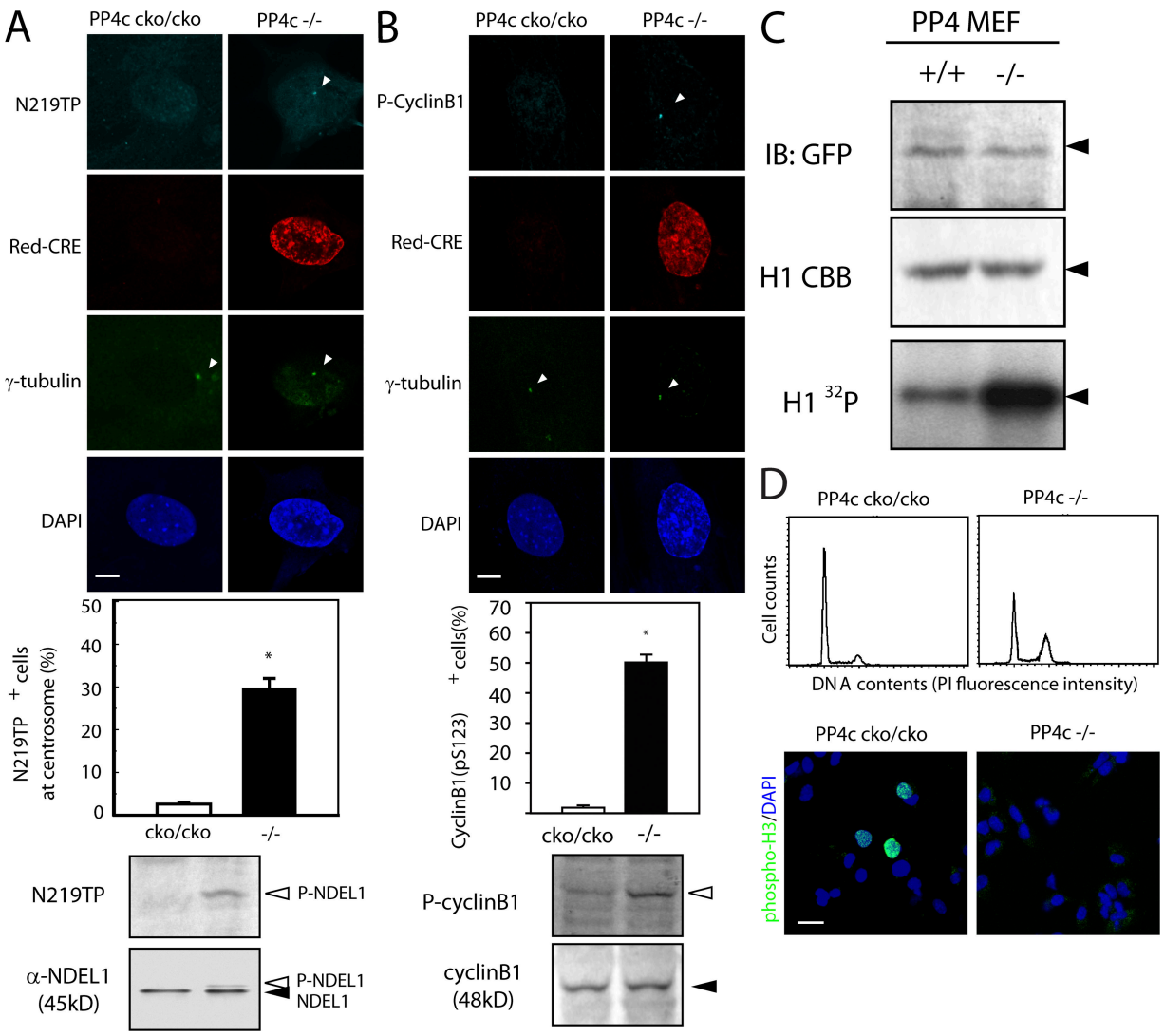

Figure 4. **Unscheduled activation of Cdk1 in *PP4c*$^{-/-}$ MEF cells.** (A) Aberrant phosphorylation at T219 of NDEL1 in *PP4c*$^{-/-}$ MEF cells (48 h after infection of *PP4c*$^{cko/cko}$ MEF cells with *adeno-Cre*). Uninfected *PP4c*$^{cko/cko}$ MEF cells were used as controls. (top) T219-phosphorylated NDEL1 was detected by using a phospho-T219–specific monoclonal antibody (N219TP). Arrowheads indicate aberrant N219TP staining and γ-tubulin of *PP4c*$^{-/-}$ MEF cells in interphase. (middle) Statistical analysis of N219TP-positive cells in interphase (*, P < 0.001; one example of three independent experiments; *n* = 100). (bottom) Western blotting pattern using a phospho-T219–specific monoclonal antibody. An anti-NDEL1 antibody was used for a control. Note that phosphorylated NDEL1 displayed lower mobility. (B) Unscheduled phosphorylation of cyclin B1 of *PP4c*$^{-/-}$ MEF cells in interphase 48 h after infection of *PP4c*$^{cko/cko}$ MEF cells with *adeno-Cre*. Uninfected *PP4c*$^{cko/cko}$ MEF cells were used as controls. (top) Antiphospho–cyclin B1 (phospho-S123) staining in *PP4c*$^{-/-}$ MEF cells. (middle) Statistical analysis of phospho-S123–positive cells (*, P < 0.001; one example of three independent experiments; *n* = 100). Error bars represent SEM. (bottom) Western blotting pattern using an antiphospho–cyclin B1–specific monoclonal antibody. An anti–cyclin B1 antibody was used for a control. (A and B) Arrowheads indicate the positions of centrosomes. (C) Histone H1 kinase assay. GFP-PACT-Cdk1 and Red-Cre plasmids were transfected to *PP4c*$^{+/+}$ or *PP4c*$^{cko/cko}$ MEF cells. GFP-PACT-Cdk1 was precipitated by an anti-GFP antibody 48 h after transfection followed by a kinase assay using histone H1 as a substrate. Note that GFP-PACT-Cdk1 extracted from *PP4c*$^{-/-}$ MEF cells displayed higher kinase activity. (D) Flow cytometric analysis of *PP4c*$^{-/-}$ MEF cells (top) and immunostaining pattern using an antiphosphohistone H3 antibody (bottom) 48 h after infection of *PP4c*$^{cko/cko}$ MEF cells with *adeno-Cre*. Uninfected *PP4c*$^{cko/cko}$ MEF cells were used as controls. Although flow cytometry revealed the enrichment of cell populations in 2n and 4c, phosphohistone H3–positive cells were rarely detected, suggesting that most of the population of *PP4c*$^{-/-}$ MEF cells was arrested in G2 before entering into prophase. One example of three independent experiments is shown. Bars, 10 μm.

PP4c$^{-/-}$ MEF cells displayed abnormal accumulation of p60 and perturbations of MT dynamics

We demonstrated that the disruption of *PP4c* results in abnormal T219 phosphorylation of NDEL1 and centrosomal recruitment of katanin p60. Oligomerization of katanin p60 increased the affinity of katanin for MTs and stimulated its ATPase activity (McNally and Vale, 1993; Hartman et al., 1998). Therefore, excessive concentration of katanin p60 at the centrosome might enhance the severing of MTs. To evaluate the nucleation of MTs at the centrosome, we performed the MT regrowth assay after total depolymerization of MTs by nocodazole treatment (Abal et al., 2002). After 5 min of recovery from the nocodazole treatment, newly synthesized MTs radiated from the centrosome in *PP4c*$^{cko/cko}$ MEF cells (Fig. 6 A). In contrast, *PP4c*$^{-/-}$ MEF cells revealed severe reduction in the regrowth of MTs from the centrosome. In addition, MTs did not create long fibers. These observations suggest that loss of PP4c might cause a nucleation defect of MTs and/or loss of stability of MT array from the centrosome.

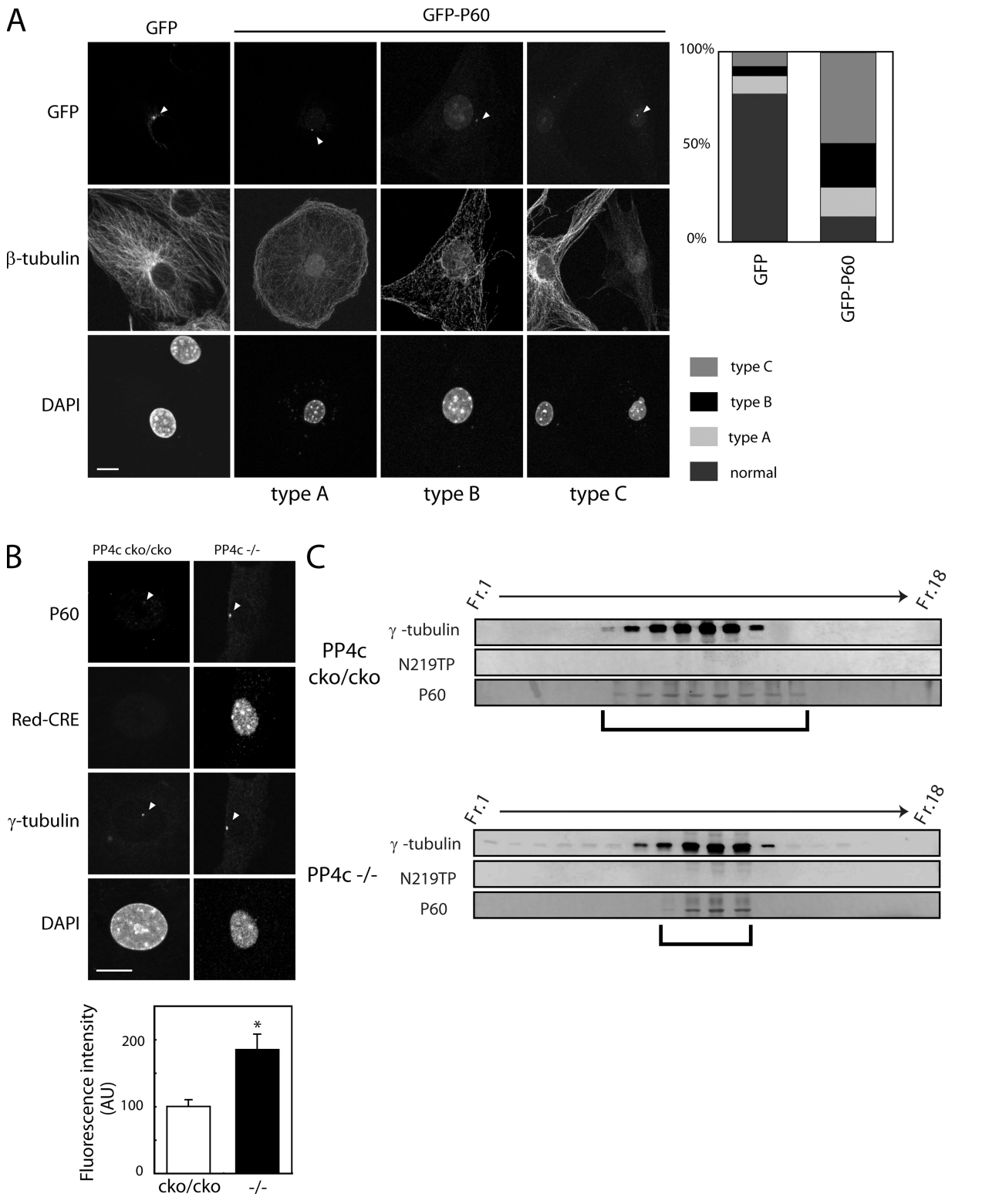

Figure 5. **Abnormal accumulation of katanin p60 in *PP4c*$^{-/-}$ MEF cells.** (A) Overexpression of katanin p60 in MEFs resulted in defective MT array, which was seen in *PP4c*$^{-/-}$ MEF cells. Statistical analysis was performed (right; $n = 50$ in each group). (B) Abnormal katanin p60 accumulation at the centrosome in *PP4c*$^{-/-}$ MEF cells 48 h after infection of *PP4c*$^{cko/cko}$ MEF cells with *adeno-Cre*. Uninfected *PP4c*$^{cko/cko}$ MEF cells were used as controls. (top) MEF cells of each genotype were stained with an anti–katanin p60 antibody. Fluorescence intensity was calculated using ImageJ software. (bottom) Fluorescence intensity in arbitrary units (*, $P < 0.05$; one example of three independent experiments; $n = 100$). Error bars represent SEM. (A and B) Arrowheads indicate the positions of centrosomes. (C) Immunoblotting analysis of sucrose gradient fractions of centrosomal extracts using antibodies against γ-tubulin, phospho-T-219 NDEL1, and katanin p60. Proteins were extracted from uninfected *PP4c*$^{cko/cko}$ MEF cells or *PP4c*$^{-/-}$ MEF cells 48 h after infection of *PP4c*$^{cko/cko}$ MEF cells with *adeno-Cre* and were subjected to sucrose density gradient fractionations. One example of three independent experiments is shown. Note the presence of phosphorylated NDEL1 with γ-tubulin in *PP4c*$^{-/-}$ MEF cells and a more restricted distribution of katanin p60 in the central fractions with phosphorylated NDEL1. Bars, 10 μm.

To visualize the MT dynamics in living cells, we used EB1-GFP as a marker of growing distal tips of MTs (Mimori-Kiyosue et al., 2000) using optical scanning microscopy (see Materials and methods). In the *PP4c*$^{cko/cko}$ MEF cells, the great majority of EB1-GFP dots emanated from the centrosome and spread throughout the cytoplasm (Video 1, available at http://www.jcb.org/cgi/content/full/jcb.200705148/DC1). In contrast, *PP4c*$^{-/-}$ MEF cells displayed fewer EB1-GFP foci moving away from the centrosome, which is associated with an intense signal of EB1-GFP around the centrosome, suggesting that these cells carry unusually large amounts of MT plus ends close to the centrosome (Fig. 6, B and C; and Video 2). EB1-GFP foci emanating from the centrosome in *PP4c*$^{-/-}$ MEF cells were growing at a relatively normal speed, implying that loss of PP4c does not perturb the assembly of tubulins. Quantitative analysis of the fluorescence intensity of EB1-GFP at the centrosome in *PP4c*$^{-/-}$ MEF cells indicated that *PP4c* disruption caused a twofold increase in EB1-GFP at the centrosome compared with *PP4c*$^{cko/cko}$ MEF cells (Fig. 6 D). In contrast, the number of MT plus ends in the cytoplasm, which was determined by counting EB1-GFP spots, was reduced by ~45% in *PP4c*$^{-/-}$ MEF cells compared with *PP4c*$^{cko/cko}$ MEF cells (Fig. 6 E). The intensity of γ-tubulin was similar between normal and *PP4c*$^{-/-}$ MEF cells as shown in Fig. 3 A. These observations suggest that MTs are able to nucleate at the centrosome, but they are abnormally severed thereafter in *PP4c*$^{-/-}$ MEF cells. Free MT minus ends would likely be unstable in *PP4c*$^{-/-}$ MEF cells; thus, fragmentation could lead to an overall reduction in the number of astral MTs (Rodionov et al., 1999). This would provide an explanation for the reduction of EB1 signal in the cytoplasm in *PP4c*$^{-/-}$ MEF cells.

To examine the perturbations in MT dynamics caused by the loss of PP4c, we transiently expressed GFP-tubulin. Because of the high density and complex organization of MTs in the vicinity of the centrosome, monitoring individual dynamics of MTs in MEF cells is technically challenging. Therefore, we analyzed the time course of MT organization in the peripheral region of the cell (Table 1). The reduced number of MTs in these basal patches allowed us to identify MT distributions and activities that contribute to the organization of MT networks. In types B and C, *PP4c*$^{-/-}$ MEF cells displayed a severe fragmentation of MTs, which made it impossible to define MTs connecting to the centrosome. Therefore, we selected *PP4c*$^{-/-}$ MEF cells from type A, which allowed us to find MTs connected to the centrosome. In *PP4c*$^{cko/cko}$ MEF cells, dynamic MTs grew steadily and radially toward the periphery. Derived from the instantaneous rates of dynamic instability, the growth rate and the shrink rate were 10.31 ± 0.65 μm/min and 17.93 ± 1.11 μm/min, respectively (Table I). As growing MTs reached cell margins, the majority initiated episodes of typically 10–20 s of pausing followed by rapid shortening (catastrophes) and regrowth (rescues), preserving the radial orientation of most MTs. In contrast, *PP4c*$^{-/-}$ MEF cells failed to undergo growth, exhibiting 43% less time in growth and 34% more time in pausing. *PP4c*$^{-/-}$ MEF cells exhibited 1.6-fold more episodes of catastrophic shortening, whereas the rescue frequency was similar. Despite the noticeable differences in MT dynamics, actual rates of MT growth and shrinkage were similar between *PP4c*$^{cko/cko}$ MEF cells and *PP4c*$^{-/-}$ MEF cells.

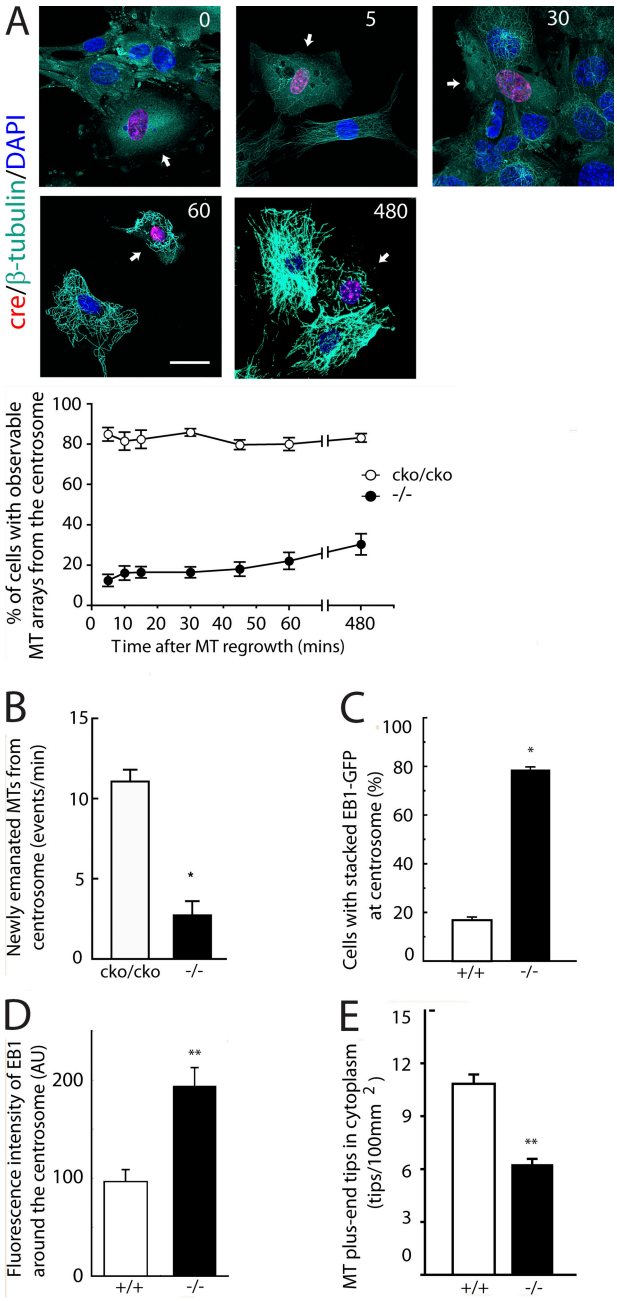

Figure 6. **Examination of MT dynamics in *PP4c*$^{-/-}$ MEF cells.** (A) Impairment of MT stability at the centrosome after nucleation in *PP4c*$^{-/-}$ MEF cells 48 h after infection of *PP4c*$^{cko/cko}$ MEF cells with *adeno-Cre*. Time (given in seconds) after washout of nocodazole is indicated in the top right corners. Arrows indicate Cre-positive cells. (top) β-Tubulin staining after MT regrowth in *PP4c*$^{cko/cko}$ MEF cells (DAPI staining only) and *PP4c*$^{-/-}$ MEF cells (arrows indicate DAPI and RFP-Cre positive). (bottom) Statistical analysis of the percentage of cells with observable MT array from the centrosome (n = 200 for each time point of each genotype). (B) Statistical analysis of the newly emanated MTs from the centrosome (*, $P < 0.001$; n = 12 for *PP4c*$^{cko/cko}$ MEF cells and n = 20 for *PP4c*$^{-/-}$ MEF cells). (C) Statistical analysis of the number of cells with stacked EB1-GFP at the centrosome (*, $P < 0.001$; one example of three independent experiments; n = 50). (D) Statistical analysis of fluorescence intensity (in arbitrary units) of EB1-GFP at the centrosome is shown (**, $P < 0.05$; n = 30 for each genotype). (E) Statistical analysis of the number of plus end tips of MTs in the cytoplasm. We calculated the number of EB1-GFP spots per 100 μm^2 area in the fixed MEF cells (**, $P < 0.05$; n = 30 for each genotype). Error bars represent SEM. Bars, 20 μm.

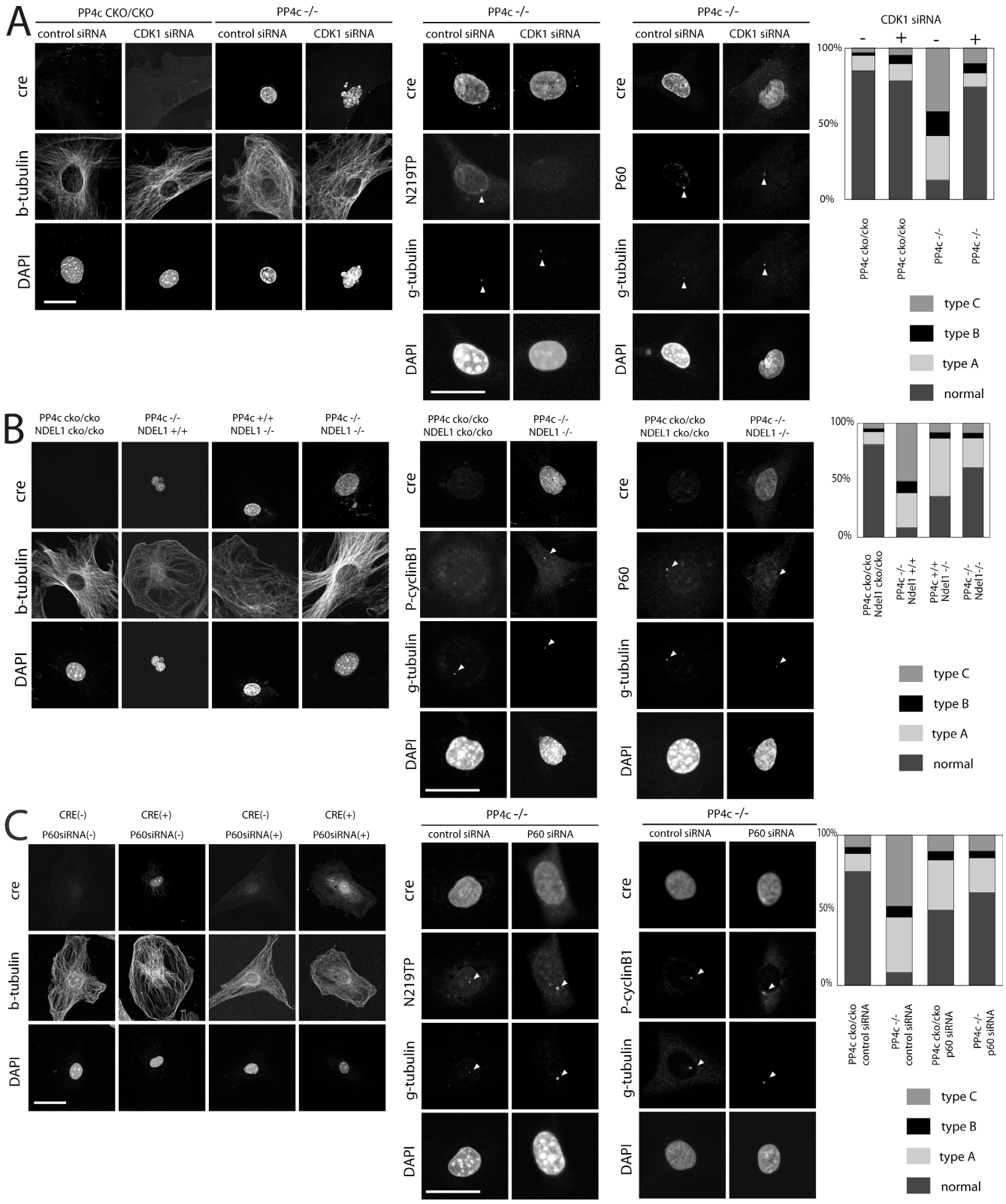

Figure 7. **Rescue experiments in PP4c-disrupted MEF cells by a Cdk1 inhibitor, additional disruption of *Ndel1*, and siRNA against katanin p60.** (A) Depletion of Cdk1 by siRNA rescued the defect of MTs in *PP4c*$^{-/-}$ MEF cells (type A). (left) MT array was rescued by the depletion of Cdk1. (middle) T219 phosphorylation of NDEL1 (left) and katanin p60 distribution (right) under control siRNA or Cdk1 siRNA in *PP4c*$^{-/-}$ MEF cells (RFP-Cre positive). One example of three independent experiments is shown. (right) Statistical analysis of the effect of Cdk1 inhibition on MT defects (n = 200 for each of *PP4c*$^{cko/cko}$; control siRNA, *PP4c*$^{cko/cko}$; Cdk1 siRNA, *PP4c*$^{-/-}$; control siRNA, and *PP4c*$^{-/-}$; Cdk1 siRNA). (B) *Ndel1* deletion can rescue the defect of MTs in *PP4c*$^{-/-}$ MEF cells (type A). (left) *PP4c*$^{-/-}$/*Ndel1*$^{-/-}$ MEF cells show a normal MT array compared with *PP4c*$^{-/-}$/*Ndel1*$^{+/+}$ MEF cells. (middle) S123 phosphorylation of cyclin B1 (left) and katanin p60 distribution (right) in *PP4c*$^{cko/cko}$/*Ndel1*$^{cko/cko}$ MEF cells (RFP-Cre negative) or *PP4c*$^{-/-}$/*Ndel1*$^{-/-}$ MEF cells (RFP-Cre positive). One example of three independent experiments is shown. (right) Statistical analysis of the effect of *Ndel1* deletion on MT abnormality (n = 100 for each of

Table I. **Quantitation of MT dynamic behavior in PP4c$^{-/-}$ MEFs**

Used MEF transfection	CKO/CKO	PP4c$^{-/-}$	PP4$^{CKO/CKO}$ control RNAi	PP4$^{CKO/CKO}$ p60 RNAi	PP4$^{CKO/CKO}$ p60 MT	PP4c$^{-/-}$ control RNAi	PP4c$^{-/-}$ p60 RNAi	PP4c$^{-/-}$ p60 MT
Growth rate (mm/min)	10.31 ± 0.65	13.62 ± 0.88	11.74 ± 0.45	14.32 ± 0.57	13.89 ± 0.33	13.20 ± 0.47	13.63 ± 0.34	13.50 ± 0.48
Shrink rate (mm/min)	17.93 ± 1.11	20.29 ± 1.29	18.54 ± 1.63	17.82 ± 0.53	17.14 ± 0.92	19.83 ± 1.15	18.89 ± 0.65	18.23 ± 1.90
Percent time spent								
Growth	30.7	17.5	25.5	56.3	41.2	13.4	34.3	30.2
Shrink	20.1	16.2	18.2	22.2	21.6	13.4	21.7	20.1
Pause	49.2	66.3	56.3	24.2	37.2	73.2	44	49.7
Catastrophe frequency (min^{-1})	0.98 ± 0.09	1.60 ± 1.10	1.03 ± 0.12	1.37 ± 0.18	1.44 ± 0.09	1.70 ± 0.07	1.05 ± 0.07	1.05 ± 0.10
Rescue frequency (min^{-1})	1.78 ± 0.10	1.65 ± 0.08	1.69 ± 0.12	1.93 ± 0.14	1.94 ± 0.07	1.59 ± 0.10	1.91 ± 0.08	2.04 ± 0.29
No. of MTs	146	153	160	122	108	102	140	138
No. of cells	11	14	14	13	10	8	9	12

p60 RNAi, siRNA against katanin p60; p60 MT, katanin p60 mutated plasmid. We selected type A PP4c2/2 MEF for examination.

Inhibition of Cdk1, additional disruption of *Ndel1*, or suppression of katanin p60 can rescue the disorganization of MTs in *PP4c*$^{-/-}$ MEF cells

We found that *PP4c* disruption results in the increased phosphorylation of T219 of NDEL1 accompanied by the unscheduled activation of Cdk1 in interphase. *PP4c*$^{-/-}$ MEF cells revealed fragmented MTs near the centrosome. Therefore, we reasoned that perturbations of MTs in *PP4c*$^{-/-}$ MEF cells could, in part, be caused by an increase in katanin p60 levels at the centrosome, which could be relieved by inhibition of Cdk1, additional disruption of *Ndel1*, or suppression of katanin p60 activity.

First, to explore the causative relationships between the unscheduled activation of Cdk1 and disorganization of MTs, we used an siRNA knockdown approach to inactivate Cdk1 (Fig. 7 A and Fig. S5 A, available at http://www.jcb.org/cgi/content/full/jcb.200705148/DC1). Silencing of Cdk1 clearly suppressed the phosphorylation of NDEL1 at T219, which lead to the reduction of katanin p60 recruitment to the centrosome, resulting in an improvement of MT organization. As another method to inhibit Cdk1 activity, *PP4c*$^{-/-}$ MEF cells were cultured in the presence of the Cdk inhibitor butyrolactone I (Fig. S5 B; Kitagawa et al., 1993). Inhibition of Cdk1 suppressed the phosphorylation of NDEL1 at T219 and facilitated the redistribution of katanin p60 from the centrosome to the cytoplasm, resulting in a reduction of katanin p60 concentration at the centrosome. As with Cdk1 siRNA, butyrolactone I resulted in an improvement of the MT organization in *PP4c*$^{-/-}$ MEF cells (Fig. S5 B). These observations suggest that abnormal activation of Cdk1 may be a causative mechanism for abnormal katanin p60 accumulation at the centrosome.

Second, we addressed whether double disruption of *PP4* and *Ndel1* can rescue MT disorganization. We mated *PP4c*$^{cko/cko}$ mice and *Ndel1*$^{cko/cko}$ mice (Sasaki et al., 2005) and generated *PP4c*$^{cko/cko}$/*Ndel1*$^{cko/cko}$ mice. *PP4c*$^{cko/cko}$/*Ndel1*$^{cko/cko}$ mice are viable and fertile, and we established MEF cell lines from embryos of these mice. We previously reported that the disruption of *Ndel1* resulted in a mislocalization of katanin p60 into the nucleus (Toyo-Oka et al., 2005). In double mutants, katanin p60 displayed diffuse distribution involving the nucleus rather than a centrosomal distribution despite the presence of activated Cdk1 (Fig. 7 B). Importantly, the centrosomal array of MTs was clearly improved. Our findings suggest that NDEL1 is located in the middle of the pathway between PP4c and katanin p60.

Finally, we examined whether depletion of katanin p60 by RNA interference or expression of dominant-negative katanin p60 can rescue MT disorganization (Fig. S5 C). In katanin p60–depleted *PP4c*$^{cko/cko}$ MEF cells, MTs exhibited twofold less time in pausing and longer periods of growth (Table 1). In addition, the growth rate was clearly augmented. The behavior of MTs also revealed that these MTs continued to grow, bending and curling at margins instead of tethering transiently to the membrane. Consistent with this feature, many MTs in katanin p60–depleted cells appeared to be longer than their counterparts. Interestingly, in these cells, MTs revealed more frequent episodes of catastrophic shortening. Most importantly, however, perturbation of MT nucleation in *PP4c*$^{-/-}$ MEF cells was clearly rescued by the depletion of katanin p60 (Fig. 7 C). In addition, the extended pause of MTs and augmented episodes of catastrophe were also relieved (Table 1). Depletion of katanin p60 in *PP4c*$^{-/-}$ MEF cells did not suppress the unscheduled activation of Cdk1 and did not inhibit the abnormal phosphorylation of T219 of NDEL1 (Fig. 7 C). Next, we tested whether the expression of dominant-negative katanin p60 is able to rescue MT defects in *PP4c*$^{-/-}$ MEF cells (Fig. S5 D; Buster et al., 2002). The expression of dominant-negative p60 in wild-type cells had

PP4c$^{cko/cko}$/*Ndel1*$^{cko/cko}$, *PP4c*$^{-/-}$/*Ndel1*$^{+/+}$, *PP4c*$^{+/+}$/*Ndel1*$^{-/-}$, and *PP4c*$^{-/-}$/*Ndel1*$^{-/-}$). (C) Rescue experiments with siRNA against katanin p60 in *PP4c*$^{-/-}$ MEF cells (type A). (left) Depletion of katanin p60–rescued MT defects in *PP4c*$^{-/-}$ MEF cells. (middle) Depletion of katanin p60 did not prevent the aberrant NDEL1 phosphorylation (left) and the unscheduled cyclin B1 phosphorylation (right) in *PP4c*$^{-/-}$ MEF cells (RFP-Cre positive). One example of three independent experiments is shown. (right) Statistical analysis of the effect of katanin p60 depletion by siRNA against katanin p60 on MT defects (n = 200 each of Cre^{-}/ctrlRNAi^{+}, CRE^{+}/ctrlRNAi^{+}, CRE^{-}/p60RNAi^{+}, and CRE^{+}/p60RNAi^{+}). (A–C) Arrowheads indicate the positions of centrosomes. Bars, 20 µm.

a similar effect on MT dynamics as the depletion of katanin p60 by siRNA (Table 1). Importantly, the expression of dominant-negative p60 in *PP4c*$^{-/-}$ MEF cells restored MT behavior. These observations suggest that the disorganization of MT array in *PP4c*$^{-/-}$ MEF cells could be partly attributed to the accumulation of excess katanin p60 associated with the unscheduled activation of Cdk1 and the phosphorylation of NDEL1 by Cdk1.

Discussion

We have identified PP4c as an NDEL1-interacting protein. *PP4c* is a highly conserved *PP2A*-related serine/threonine phosphatase (Brewis et al., 1993) that efficiently dephosphorylates NDEL1 at Cdk1 phosphorylation sites. Interestingly, PP4c is preferentially distributed at the interphase centrosome and rapidly relocates from the centrosome upon entry into mitosis, which coincides with the activation of Cdk1 and the phosphorylation of NDEL1 by activated Cdk1. We further found that persistent expression of PP4c at the centrosome prevented the activation of Cdk1 and mitotic progression. In addition, the expression of PP4c prevented phosphorylation of NDEL1 by coexpressed active Cdk1, suggesting that PP4c is functionally dominant over Cdk1 and might be a checkpoint protein for the entrance of mitosis. Interestingly, the expression of mitotic Cdk1 in interphase facilitated the phosphorylation of NDEL1 and increased centrosomal levels of katanin p60, resulting in a reduction in MTs and suggesting that a coordination of PP4c and Cdk1 activities is essential for the proper regulation of MT organization.

To address how PP4c regulates NDEL1 at the centrosome, we have generated mice carrying a conditional KO allele of *PP4c*. *PP4c*$^{-/-}$ MEF cells exhibited a disorganized MT array associated with the reduction of centrosomal connections. Transient expression of EB1-GFP and analysis of MT dynamics revealed the significant reduction of emanation of MTs from the centrosome. EB1 also accumulated at the centrosome and was reduced within the cytoplasm in *PP4c*$^{-/-}$ MEF cells. We propose that EB1 behavior in *PP4c*$^{-/-}$ MEF cells is attributable to the increased severing activity of MTs at the centrosome. This would explain the accumulation of EB1 at the centrosome. A failure of MT connection to the centrosome is known to cause MT instability (Rodionov et al., 1999), which would result in a reduction of EB1 signal in the cytoplasm. We also examined MT behaviors using GFP-tubulin. In *PP4c*$^{-/-}$ MEF cells, MTs were prone to stay paused with reduced growth. Catastrophe frequency was markedly increased in *PP4c*$^{-/-}$ MEF cells. In addition, MT dynamics in *PP4c*$^{-/-}$ MEF cells were similar both at the cell periphery and around the centrosome. Taking this into account, we speculate that these MT behaviors would reflect an event at the centrosome, presumably the frequent loss of MT connection with the centrosome. Interestingly, *PP4c* disruption resulted in the unscheduled activation of Cdk1 and aberrant phosphorylation of NDEL1, which is associated with the excessive recruitment of katanin p60 at the centrosome. These findings suggest that PP4c may regulate the distribution of katanin p60 through regulation of Cdk1 activity and phosphorylation/dephosphorylation of NDEL1. Excessive katanin p60 at the centrosome would partly explain the frequent loss of MT connection with the centrosome in *PP4c*$^{-/-}$ MEF cells. We found increased levels of centrosomal 14-3-3ε and decreased distribution of centrosomal dynactin 1 and differential interference contrast (unpublished data). Dynactin 1 binds to EB1, and these interactions are essential for MT anchoring at the centrosome (Berrueta et al., 1999; Askham et al., 2002). Although these additional factors would further modulate the phenotypes of MT disorganization in *PP4c*$^{-/-}$ MEF cells, we believe that abnormal accumulation of katanin p60 is a primary event. Depletion or inhibition of Cdk1 activity by siRNA or an inhibitor, additional disruption of *Ndel1*, or inhibition of katanin p60 by siRNA or dominant-negative p60 suppressed the perturbation of MT dynamics in *PP4c*$^{-/-}$ MEF cells, fully supporting our interpretation.

Recently, chromosome movement toward mitotic spindle poles by a Pacman-flux mechanism has been proposed (Zhang et al., 2007). In this model, katanin p60 appears to function primarily on anaphase chromosomes, where it stimulates MT plus end depolymerization. In our model, katanin p60 plays an essential role at the centrosome for MT remodeling. These differences might be attributable to the stage of cell cycle (mitosis or interphase) and/or the origin of cells (*Drosophila* and mammals). The prolonged growth rate of MTs by depletion of katanin p60 by siRNA or expression of dominant-negative p60 supports our interpretation.

Centrosomes are the dominant sites of MT assembly. In particular, as cells enter mitosis, centrioles recruit pericentriolar material in the process of centrosome maturation, which increases the MT nucleating capacity at the centrosomes (Doxsey et al., 2005a,b). The increased dynamics of MTs in mitosis is an essential prerequisite for spindle formation. It is driven by coordination of the activities of MT-stabilizing and -destabilizing factors. For example, the combination of XMAP215 and XKCM1/mitotic centromere-associated kinesin is essential to promote the dynamic properties of mitotic MT assembly (Tournebize et al., 2000; Kinoshita et al., 2001). The coordination of these components is further modulated by the activities of kinases and phosphatases. We previously reported that NDEL1 is essential for centrosomal targeting of katanin p60 (Toyo-Oka et al., 2005). Targeted disruption of *Ndel1* resulted in an abnormal nuclear distribution of katanin p60 and perturbation of MT organization. In addition, phosphorylation of NDEL1 by Cdk1 enhances the affinity between NDEL1 and katanin p60. We recently reported that NDEL1 is phosphorylated by Aurora A and is required for recruitment of TACC3 to the centrosome (Mori et al., 2007). Phosphorylation of NDEL1 by Cdk1 may contribute to the destabilization of MT connections at the centrosome by recruitment of katanin p60. Conversely, phosphorylation of NDEL1 by Aurora A may influence the stabilizing machinery by accentuating the localization of TACC3 at the centrosome. PP4c contributes to regulation of the proper activation of Cdk1 and recruitment of katanin p60 at the centrosome. The MT behavior in *PP4c*$^{-/-}$ MEF cells leads us to speculate that PP4c may be a part of the regulatory machinery for the MT-stabilizing pathway, acting directly/indirectly through the regulation of centrosomal components, including Cdk1, NDEL1, and katanin p60. Our observations underscore the importance of NDEL1 in the recruitment and coordination of centrosomal components.

In addition, maintenance of the proper phosphorylation of NDEL1 is essential for the regulation of MT dynamics by recruitment of proper target molecules.

Materials and methods

Yeast two-hybrid screening and in vitro dephosphorylation activity
Full-length *Ndel1* cDNA was conjugated to *pLexA* (Clontech Laboratories, Inc.) and used to screen a fetal mouse brain cDNA yeast two-hybrid library as described previously (Sasaki et al., 2000). Although protein interaction was confirmed by a yeast two-hybrid analysis, direct interaction was not detected by an immunoprecipitation assay, suggesting that the enzyme–substrate interaction might not be strong enough for the detection of protein interaction by nonequilibrium binding assays. We generated GST-tagged full-length recombinant NDEL1 (Toyo-Oka et al., 2005), cyclin B1, Cdk1, Aurora A (Marumoto et al., 2003), and PP4c by Bac-to-Bac baculo-system (Invitrogen) using SF-9 or High Five insect cells (BD Biosciences). To obtain active Cdk1, baculovirus carrying GST–cyclin B1 and GST-Cdk1 were simultaneously inoculated to High Five insect cells. Recombinant proteins were purified using GST-Sepharose (GE Healthcare), and the GST tag of NDEL1 was removed by thrombin digestion (GE Healthcare) based on the manufacturer's manual. A mutated *GST-PP4c* construct in which arginine 236 was replaced with leucine, resulting in a loss of phosphatase activity (Zhou et al., 2002), was generated by QuikChange (Stratagene). NDEL1 was phosphorylated by GST-Cdk1 or GST–Aurora A as reported previously (Mori et al., 2007). Kinases and unincorporated ATP were removed by GST column and gel filtration column (GE Healthcare). Dephosphorylation assays of NDEL1 by GST-PP4c were performed in a 50-µl reaction mixture containing 0.1 µg of phosphorylated NDEL1, 20 mM Tris-HCl, pH 7.4, 1 mM DTT, and 1 mM EDTA. After incubation at 30°C for 20 min, the reaction was terminated and subjected to SDS-PAGE followed by autoradiography.

Generation of *PP4c* knockout mice and MEF cell line
We generated a conditional knockout mouse to inactivate *PP4c* by Cre-mediated recombination. We assembled a targeting construct in which a loxP site and a *PGK-neo* gene flanked by two loxP sites were inserted into intron IV and downstream of *PP4c*, respectively. The linearized targeting construct was introduced into TC1 embryonic stem cells (Deng et al., 1996) from a 129S6 background by electroporation. The targeted embryonic stem clones were screened by Southern blotting and injected into blastocysts to create chimeric mice. Highly agouti chimeric males were mated to wild-type females to give rise to heterozygotes for $PP4c^{neo/+}$, which were identified by Southern blot analysis and PCR. These heterozygous mice were mated with *EIIa-Cre* germline deleter transgenic mice (Lakso et al., 1996). Offsprings from the matings between a $PP4c^{neo/+}$ line and an *EIIa-Cre* transgenic line were genotyped by Southern blot analysis and PCR. The Southern blot analysis and PCR examination indicated deletion of the fragment carrying exons V–VIII by Cre-mediated recombination in vivo ($PP4c^{-/+}$). $PP4c^{neo/neo}$ mice revealed embryonic lethality, suggesting that the presence of the *neo* gene affects the expression of *PP4c*. To generate $PP4c^{cko/+}$, we mated a $PP4c^{neo/+}$ line with an *EIIa-Cre* transgenic line and isolated offsprings in which only loxp-flanked *PGK-neo* was removed by Cre-mediated partial recombination. $PP4c^{cko/cko}$ mice were generated by the mating of $PP4c^{cko/+}$ and turned out to be viable, fertile, and able to be maintained as homozygotes. $PP4c^{cko/cko}$ MEF cells were established from embryonic day 12.5 embryos from matings of $PP4c^{cko/cko}$. We also established $PP4c^{+/+}$ MEF cells from embryonic day 12.5 embryos from matings of wild-type mice. These MEF cell lines were transfected with each plasmid or infected with adenovirus carrying a *Cre* gene (*adeno-Cre*) and were subjected to live imaging or immunostaining at given times after transfection. $PP4c^{+/+}$ MEF cells were used for controls as the same condition.

To quantify fluorescence intensity, centrosomes were surrounded by a 0.5-µm-diameter circle, and fluorescence intensity of the circle was measured. We also measured background intensity close to the centrosome with the same diameter circle and subtracted the background intensity from the centrosomal intensity in each case.

Generation of expression constructs
To make expression vectors, we cloned each cDNA into *pEGFP* (Clontech Laboratories, Inc.). Phosphatase-inactive *PP4c* and mitotic *Cdk1* were generated by QuikChange (Zhou et al., 2002; Litvak et al., 2004). For the *Cre* expression vector, the *Cre* gene was conjugated to a *Cherry* vector. To achieve centrosome-restricted expression of *PP4c* or *Cdk1*, we conjugated each protein to a PACT domain derived from pericentrin (Gillingham and Munro, 2000). Dominant-negative *katanin p60* used in the experiments was reported previously (Toyo-Oka et al., 2005).

Generation of the antibodies against PP4, R1, and phosphorylated mouse cyclin B1 (phospho-S123)
To make anti-PP4c or R1 antibodies, we immunized New Zealand white rabbits with a GST-conjugated recombinant PP4c (1–55 amino acids) or R1 (452–622 amino acids) expressed in bacteria and purified by GST-Sepharose according to standard procedures. The antisera against PP4c-(1–55 amino acids) or R1 (452–622 amino acids)-peptide were collected and purified by HiTrap columns (GE Healthcare) coupled with the antigens used (PP4c [1–55 amino acids] or R1 [452–622 amino acids]). To produce antiphosphorylated mouse cyclin B1 (phospho-S123) antibody, keyhole limpet hemocyanin (KLH)–conjugated mouse cyclin B1 phosphopeptides (CILVDNP[pS]PSPME) were injected into New Zealand white rabbits according to standard procedures. The antisera were first applied to KLH-conjugated nonphosphorylated peptides (CILVDNPSPSPME) to remove anti-KLH antibodies and antibodies that bind to nonphosphorylated peptides and were purified by using phosphopeptide (CILVDNP[pS]PSPME)-coupled HiTrap columns.

Cell culture, transfection, and synchronization of HeLa cells
HeLa cells were cultured in MEM (Sigma-Aldrich) supplemented with 10% FCS. For mitosis synchronization, HeLa cells were exposed to 2 mM thymidine for 16 h and were resuspended in fresh medium supplemented with 24 µM 2′-deoxycytidine and allowed to grow for 9 h. 2 mM thymidine was added again for 16 h, causing cells to accumulate near the G1/S boundary. MEF cells were prepared from various conditional knockout mouse embryos according to standard procedure. MEF cells were grown in DME supplemented with 10% FBS and penicillin/streptomycin. For transfection, cells were collected by using 0.25% trypsin/1 mM EDTA in HBSS and transfected with the Nucleofector transfection system (Amaxa) with a MEF1 kit according to the manufacturer's instructions. For immunostaining, cells were plated onto eight-well chamber slides (BD Biosciences) at a density of $1–2 \times 10^4$ cells/well after transfection. For time-lapse imaging, cells were plated onto four-well LabTekII chamber slides (coverslip bottom; Thermo Fisher Scientific) at a density of $1–1.5 \times 10^5$ cells/well after transfection. Cells were used for experiments 24–48 h after transfection. For the analysis of MT dynamics, cells were treated with 0.3 U/ml Oxyrase oxygen scavenging system (EC Oxyrase) to reduce photodamage and photobleaching (Mikhailov and Gundersen, 1995). The Oxyrase-treated cells were covered with mineral oil to prevent gas exchange.

Construction of recombinant adenoviruses
Recombinant adenoviruses (Ad-FRP-Cre) were constructed according to the manufacturer's instructions (BD Biosciences). In brief, cDNAs encoding an RFP-Cre were inserted into the pShuttle2 vector. The expression cassette was excised from the recombinant pShuttle2 plasmid DNA by digesting with I-CeuI and PI-SceI. Afterward, the expression cassette ligated to Adeno-X viral DNA (BD Biosciences). These adenoviral vectors were transfected into human embryonic kidney 293 cells, which provide the E1A gene product necessary for viral replication. The resultant recombinant viruses were propagated in 293 cells, and titers were determined by the Adeno-X Rapid titer kit (BD Biosciences).

Immunostaining
Cells were fixed in cold methanol for 3 min at −20°C or 4% PFA/PBS for 3 min at room temperature. Fixed cells were incubated with 0.2% Triton X-100/TBS to be permeabilized for 10 min at room temperature followed by blocking treatment. 5% BSA/0.2% Tween 20/TBS or milk-based blocking reagent Blockace (Dainippon Sumitomo Pharma) supplemented with 2% FCS was used for blocking an antiphosphorylated or anti-unphosphorylated protein antibody, respectively. After blocking, we incubated the cells with various antibodies at 4°C overnight or for 1 h at room temperature. We used the antibodies at the following dilutions in blocking solution: rabbit anti-NDEL1 at 1:200; 7 µg/ml affinity-purified rabbit anti-p60; 7 µg/ml affinity-purified rabbit anti-p80; 2 µg/ml affinity-purified rabbit anti-PP4c; 2 µg/ml affinity-purified rabbit anti-PP4R1; 2 µg/ml mouse monoclonal anti-T219 phosphorylated NDEL1 (clone N219TP; MBL International); rabbit anti–γ-tubulin (BioLegend) at 1:400; mouse monoclonal anti-T219 phosphorylated NDEL1 at 1:25 (clone 5; BD Biosciences); mouse monoclonal anti–β-tubulin at 1:300 (clone TUB21; Sigma-Aldrich); mouse monoclonal anti–γ-tubulin at 1:200 (clone GTU88; Sigma-Aldrich); mouse monoclonal antiacetylated tubulin at 1:100 (clone 6-11B-1; Sigma-Aldrich); rabbit anti-NDEL1 at 1:200; and 2 µg/ml affinity-purified rabbit

antiphosphorylated mouse cyclin B1 (phospho-S123) antibody. After washing three times with 0.1% Tween 20/TBS for 10 min each, cells were treated with various secondary antibodies in blocking solution for 30 min at room temperature. We used the following secondary antibodies: Cy5-labeled donkey anti–mouse IgG at 1:500 or anti–rabbit IgG at 1:400 (Jackson ImmunoResearch Laboratories) and AlexaFluor488-labeled donkey anti–mouse IgG at 1:200 or anti–rabbit IgG at 1:400 (Invitrogen). We visualized nuclei with 300 nM DAPI and mounted the cells with 90% glycerol/PBS.

Image acquisition

Images of cells were acquired with a laser-scanning confocal microscope (LSM510 version 2.3; Carl Zeiss, Inc.) or an optical sectioning microscope (DeltaVision version 2.50; Applied Precision) equipped with Axiovert plan Apochromat (63× 1.40 NA or 100× 1.40 NA; Carl Zeiss, Inc.) oil immersion or UPlanApo (20× 0.70 NA dry, PlanApo 60×1.40 NA oil, or PlanApo 100× 1.40 NA oil immersion; Olympus) objectives, respectively. Using the confocal microscope, images were recorded using confocal software (Carl Zeiss, Inc.) and were exported as TIFF. Figures were then generated using Photoshop 7.0 and Illustrator CS2 (Adobe). Using the DeltaVision system, images were acquired through a cooled CCD camera (series 300 CH350; Photometrics) with appropriate neutral density filters, binning of pixels, exposure times, and time intervals. Fluorescent signals were visualized using an Endow GFP bandpass emission filter set (model 41 017) or a Sedat Quad filter set (model 86 000; Chroma Technology Corp.). Pixel positions, distances, and areas were measured on the digital images using the analysis function of the DeltaVision Aquacosmos software (Hamamatsu) or MetaMorph software (MDS Analytical Technologies). Cell areas were quantified using the particle analysis function of the Aquacosmos software.

Analysis of MT dynamics

Obtained images were exported as TIFF files and processed with ImageJ version 1.37h (National Institutes of Health). Black and white raw data were converted to color images to visualize EB1-GFP and the end of MTs easily and were processed with the bandpass filter function of ImageJ software to remove haze. EB1-GFP and the end of MTs were traced by a mouse-driven cursor under ImageJ software plugged in the manual track function (developed and programmed by Fabrice Cordelières, Institut Curie, Orsay, France). Changes >0.5 µm between two points were considered as growth or shortening events. Changes <0.5 µm were considered as a pause. More than 100 MTs from 8–14 cells were analyzed. The results are indicated as the mean and SEM, and at least three independent experiments were performed. The frequency of catastrophe or rescue was determined as previously described (Rusan et al., 2001). In brief, the frequency of catastrophe was determined by dividing the number of transitions from growth to shortening and from pause to shortening by the time spent in growth or pause. The frequency of rescue was calculated by dividing the number of transitions from shortening to growth and from shortening to pause by the time spent shortening. MTs that could be traced for >1 min were included in the analysis. Statistical analysis was performed by using Prism software (GraphPad).

siRNA

21-nucleotide RNAs were chemically synthesized by Dharmacon Research and transfected with Lipofectamine 2000 reagents (Invitrogen) or the Nucleofector transfection system. The target sequences used were GGACAUAGAUGAGGCUUUATT and CAGAGAACAUGGAAGGCUATT against mouse *katanin p60* and GGAGUGCCCAGUACUGCAATT against mouse Cdk1. Certified control siRNA (UUCUUCGAACGUGUCACGUTT) was used as a negative control (QIAGEN). Cell lysates were prepared and analyzed for the silencing. In addition, COS7 cells expressing GFP-tagged mouse *katanin p60* (*GFP-p60*) were treated with siRNA and verified that two siRNAs down-regulated the expression of GFP-p60 (Fig. S5 C).

MT regrowth assay

The MT regrowth assay was performed as previously reported (Fry et al., 1998). In brief, RFP-Cre–transfected cells were seeded in chamber slides and treated with 1.5 µg/ml nocodazole in prewarmed culture medium for 20 min at 37°C under 5% CO_2. After washing three times with prewarmed PBS, cells were cultured with DME supplemented with 10% FBS at a given time to observe the regrowth of MTs at various points. At each time point, cells were fixed with cold methanol for 3 min followed by immunostaining with anti–β-tubulin antibody.

Online supplemental material

Fig. S1 shows the generation of a gene-disrupted mouse of *PP4c*. Fig. S2 shows the genomic organization of *PP4c* and *Tbx6*. Fig. S3 shows a characterization of an antibody against phospho-S123 of mouse cyclin B1. Fig. S4 shows a characterization of cell cycle arrest after treatment with mitomycin C or contact inhibition. Fig. S5 shows rescue experiments in *PP4c*$^{-/-}$ MEF cells. Video 1 and Video 2 show a *PP4c*$^{+/+}$ MEF cell and *PP4c*$^{-/-}$ MEF cell, respectively, undergoing emanations of EB1 from the centrosome. Online supplemental material is available at http://www.jcb.org/cgi/content/full/jcb.200705148/DC1.

We thank Virginia E. Papaioannou for providing a *Tbx6*-disrupted mouse and Mark Jackman and Jonathon Pines for providing an antiphospho–cyclin B1 antibody. We also thank Shinsuke Matsuzaki for providing a vector carrying a PACT domain, Kozo Kaibuchi for providing a GFP-EB1 construct, Takao Kenko, Emi Donoue, and Keisuke Inoue for technical support, and Hiromichi Nishimura and Keiko Fujimoto for mouse breeding. We thank Yoshihiko Funae, Toshio Yamauch, and Yoshitaka Nagai for generous support and encouragement and Virginia E. Papaioannou, Mark Jackman, Jonathon Pines, Kazuhisa Kinoshita, and Yuko Kiyosue for valuable discussion and comments.

This work was supported by Grants-in-Aid for Scientific Research from the Ministry of Education, Science, Sports and Culture of Japan to K. Toyo-oka and S. Hirotsune, by a Grant-in-Aid for Young Scientists (B) to K. Toyo-oka, and a Grant-in-Aid for Scientific Research (B) from the Ministry of Education, Science, Sports and Culture of Japan to S. Hirotsune. This work was also supported by the Yasuda Medical Research Foundation, the Cell Science Research Foundation, the Japan Spina Bifida and Hydrocephalus Research Foundation, and the Hoh-ansha Foundation (grants to S. Hirotsune) as well as by the Senri Life Science Foundation (grant to K. Toyo-oka).

Submitted: 23 May 2007
Accepted: 12 February 2008

References

Abal, M., M. Piel, V. Bouckson-Castaing, M. Mogensen, J.B. Sibarita, and M. Bornens. 2002. Microtubule release from the centrosome in migrating cells. *J. Cell Biol.* 159:731–737.

Andreassen, P.R., F.B. Lacroix, E. Villa-Moruzzi, and R.L. Margolis. 1998. Differential subcellular localization of protein phosphatase-1 α, γ1, and δ isoforms during both interphase and mitosis in mammalian cells. *J. Cell Biol.* 141:1207–1215.

Askham, J.M., K.T. Vaughan, H.V. Goodson, and E.E. Morrison. 2002. Evidence that an interaction between EB1 and p150(Glued) is required for the formation and maintenance of a radial microtubule array anchored at the centrosome. *Mol. Biol. Cell.* 13:3627–3645.

Berrueta, L., J.S. Tirnauer, S.C. Schuyler, D. Pellman, and B.E. Bierer. 1999. The APC-associated protein EB1 associates with components of the dynactin complex and cytoplasmic dynein intermediate chain. *Curr. Biol.* 9:425–428.

Blagden, S.P., and D.M. Glover. 2003. Polar expeditions–provisioning the centrosome for mitosis. *Nat. Cell Biol.* 5:505–511.

Bornens, M. 2002. Centrosome composition and microtubule anchoring mechanisms. *Curr. Opin. Cell Biol.* 14:25–34.

Brewis, N.D., A.J. Street, A.R. Prescott, and P.T. Cohen. 1993. PPX, a novel protein serine/threonine phosphatase localized to centrosomes. *EMBO J.* 12:987–996.

Buster, D., K. McNally, and F.J. McNally. 2002. Katanin inhibition prevents the redistribution of gamma-tubulin at mitosis. *J. Cell Sci.* 115:1083–1092.

Chapman, D.L., and V.E. Papaioannou. 1998. Three neural tubes in mouse embryos with mutations in the T-box gene Tbx6. *Nature.* 391:695–697.

Compton, D.A. 2000. Spindle assembly in animal cells. *Annu. Rev. Biochem.* 69:95–114.

Deng, C., A. Wynshaw-Boris, F. Zhou, A. Kuo, and P. Leder. 1996. Fibroblast growth factor receptor 3 is a negative regulator of bone growth. *Cell.* 84:911–921.

Dobyns, W.B. 1989. The neurogenetics of lissencephaly. *Neurol. Clin.* 7:89–105.

Dobyns, W.B., O. Reiner, R. Carrozzo, and D.H. Ledbetter. 1993. Lissencephaly. A human brain malformation associated with deletion of the LIS1 gene located at chromosome 17p13. *JAMA.* 270:2838–2842.

Doxsey, S. 2001. Re-evaluating centrosome function. *Nat. Rev. Mol. Cell Biol.* 2:688–698.

Doxsey, S., D. McCollum, and W. Theurkauf. 2005a. Centrosomes in cellular regulation. *Annu. Rev. Cell Dev. Biol.* 21:411–434.

Doxsey, S., W. Zimmerman, and K. Mikule. 2005b. Centrosome control of the cell cycle. *Trends Cell Biol.* 15:303–311.

Fry, A.M., P. Meraldi, and E.A. Nigg. 1998. A centrosomal function for the human Nek2 protein kinase, a member of the NIMA family of cell cycle regulators. *EMBO J.* 17:470–481.

Gillingham, A.K., and S. Munro. 2000. The PACT domain, a conserved centrosomal targeting motif in the coiled-coil proteins AKAP450 and pericentrin. *EMBO Rep.* 1:524–529.

Hartman, J.J., J. Mahr, K. McNally, K. Okawa, A. Iwamatsu, S. Thomas, S. Cheesman, J. Heuser, R.D. Vale, and F.J. McNally. 1998. Katanin, a microtubule-severing protein, is a novel AAA ATPase that targets to the centrosome using a WD40-containing subunit. *Cell.* 93:277–287.

Helps, N.R., N.D. Brewis, K. Lineruth, T. Davis, K. Kaiser, and P.T. Cohen. 1998. Protein phosphatase 4 is an essential enzyme required for organisation of microtubules at centrosomes in *Drosophila* embryos. *J. Cell Sci.* 111:1331–1340.

Hirotsune, S., M.W. Fleck, M.J. Gambello, G.J. Bix, A. Chen, G.D. Clark, D.H. Ledbetter, C.J. McBain, and A. Wynshaw-Boris. 1998. Graded reduction of Pafah1b1 (Lis1) activity results in neuronal migration defects and early embryonic lethality. *Nat. Genet.* 19:333–339.

Hu, M.C., Q. Tang-Oxley, W.R. Qiu, Y.P. Wang, K.A. Mihindukulasuriya, R. Afshar, and T.H. Tan. 1998. Protein phosphatase X interacts with c-Rel and stimulates c-Rel/nuclear factor kappaB activity. *J. Biol. Chem.* 273:33561–33565.

Jackman, M., C. Lindon, E.A. Nigg, and J. Pines. 2003. Active cyclin B1-Cdk1 first appears on centrosomes in prophase. *Nat. Cell Biol.* 5:143–148.

Kinoshita, K., I. Arnal, A. Desai, D.N. Drechsel, and A.A. Hyman. 2001. Reconstitution of physiological microtubule dynamics using purified components. *Science.* 294:1340–1343.

Kinoshita, K., B. Habermann, and A.A. Hyman. 2002. XMAP215: a key component of the dynamic microtubule cytoskeleton. *Trends Cell Biol.* 12:267–273.

Kitagawa, M., T. Okabe, H. Ogino, H. Matsumoto, I. Suzuki-Takahashi, T. Kokubo, H. Higashi, S. Saitoh, Y. Taya, H. Yasuda, et al. 1993. Butyrolactone I, a selective inhibitor of cdk2 and cdc2 kinase. *Oncogene.* 8:2425–2432.

Kloeker, S., and B.E. Wadzinski. 1999. Purification and identification of a novel subunit of protein serine/threonine phosphatase 4. *J. Biol. Chem.* 274:5339–5347.

Lakso, M., J.G. Pichel, J.R. Gorman, B. Sauer, Y. Okamoto, E. Lee, F.W. Alt, and H. Westphal. 1996. Efficient in vivo manipulation of mouse genomic sequences at the zygote stage. *Proc. Natl. Acad. Sci. USA.* 93:5860–5865.

Litvak, V., R. Argov, N. Dahan, S. Ramachandran, R. Amarilio, A. Shainskaya, and S. Lev. 2004. Mitotic phosphorylation of the peripheral Golgi protein Nir2 by Cdk1 provides a docking mechanism for Plk1 and affects cytokinesis completion. *Mol. Cell.* 14:319–330.

Marumoto, T., S. Honda, T. Hara, M. Nitta, T. Hirota, E. Kohmura, and H. Saya. 2003. Aurora-A kinase maintains the fidelity of early and late mitotic events in HeLa cells. *J. Biol. Chem.* 278:51786–51795.

McNally, F. 2000. Capturing a ring of samurai. *Nat. Cell Biol.* 2:E4–E7.

McNally, F.J., and R.D. Vale. 1993. Identification of katanin, an ATPase that severs and disassembles stable microtubules. *Cell.* 75:419–429.

Meraldi, P., and E.A. Nigg. 2001. Centrosome cohesion is regulated by a balance of kinase and phosphatase activities. *J. Cell Sci.* 114:3749–3757.

Mikhailov, A.V., and G.G. Gundersen. 1995. Centripetal transport of microtubules in motile cells. *Cell Motil. Cytoskeleton.* 32:173–186.

Mimori-Kiyosue, Y., N. Shiina, and S. Tsukita. 2000. The dynamic behavior of the APC-binding protein EB1 on the distal ends of microtubules. *Curr. Biol.* 10:865–868.

Mori, D., Y. Yano, K. Toyo-oka, N. Yoshida, M. Yamada, M. Muramatsu, D. Zhang, H. Saya, Y.Y. Toyoshima, K. Kinoshita, et al. 2007. NDEL1 phosphorylation by Aurora-A kinase is essential for centrosomal maturation, separation, and TACC3 recruitment. *Mol. Cell. Biol.* 27:352–367.

Moudjou, M., and M. Bornens. 1998. Method of centrosome isolation from cultured animal cells. *In* Cell Biology: A Laboratory Handbook. J.E. Celis, editor. Academic Press Inc., Orlando, FL. p 13.

Nigg, E.A. 2001. Mitotic kinases as regulators of cell division and its checkpoints. *Nat. Rev. Mol. Cell Biol.* 2:21–32.

Ou, Y., and J.B. Rattner. 2004. The centrosome in higher organisms: structure, composition, and duplication. *Int. Rev. Cytol.* 238:119–182.

Reiner, O., R. Carrozzo, Y. Shen, M. Wehnert, F. Faustinella, W.B. Dobyns, C.T. Caskey, and D.H. Ledbetter. 1993. Isolation of a Miller-Dieker lissencephaly gene containing G protein beta-subunit-like repeats. *Nature.* 364:717–721.

Rodionov, V., E. Nadezhdina, and G. Borisy. 1999. Centrosomal control of microtubule dynamics. *Proc. Natl. Acad. Sci. USA.* 96:115–120.

Rusan, N.M., C.J. Fagerstrom, A.M. Yvon, and P. Wadsworth. 2001. Cell cycle-dependent changes in microtubule dynamics in living cells expressing green fluorescent protein-alpha tubulin. *Mol. Biol. Cell.* 12:971–980.

Sasaki, S., A. Shionoya, M. Ishida, M.J. Gambello, J. Yingling, A. Wynshaw-Boris, and S. Hirotsune. 2000. A LIS1/NUDEL/cytoplasmic dynein heavy chain complex in the developing and adult nervous system. *Neuron.* 28:681–696.

Sasaki, S., D. Mori, K. Toyo-oka, A. Chen, L. Garrett-Beal, M. Muramatsu, S. Miyagawa, N. Hiraiwa, A. Yoshiki, A. Wynshaw-Boris, and S. Hirotsune. 2005. Complete loss of Ndel1 results in neuronal migration defects and early embryonic lethality. *Mol. Cell. Biol.* 25:7812–7827.

Shui, J.W., M.C. Hu, and T.H. Tan. 2007. Conditional knockout mice reveal an essential role of protein phosphatase 4 in thymocyte development and pre-T-cell receptor signaling. *Mol. Cell. Biol.* 27:79–91.

Thyberg, J., and S. Moskalewski. 1999. Role of microtubules in the organization of the Golgi complex. *Exp. Cell Res.* 246:263–279.

Tournebize, R., A. Popov, K. Kinoshita, A.J. Ashford, S. Rybina, A. Pozniakovsky, T.U. Mayer, C.E. Walczak, E. Karsenti, and A.A. Hyman. 2000. Control of microtubule dynamics by the antagonistic activities of XMAP215 and XKCM1 in *Xenopus* egg extracts. *Nat. Cell Biol.* 2:13–19.

Toyo-Oka, K., S. Sasaki, Y. Yano, D. Mori, T. Kobayashi, Y.Y. Toyoshima, S.M. Tokuoka, S. Ishii, T. Shimizu, M. Muramatsu, et al. 2005. Recruitment of katanin p60 by phosphorylated NDEL1, an LIS1 interacting protein, is essential for mitotic cell division and neuronal migration. *Hum. Mol. Genet.* 14:3113–3128.

Tsai, L.H., and J.G. Gleeson. 2005. Nucleokinesis in neuronal migration. *Neuron.* 46:383–388.

Vallee, R. 1991. Cytoplasmic dynein: advances in microtubule-based motility. *Trends Cell Biol.* 1:25–29.

Vallee, R.B., C. Tai, and N.E. Faulkner. 2001. LIS1: cellular function of a disease-causing gene. *Trends Cell Biol.* 11:155–160.

Walczak, C.E., T.J. Mitchison, and A. Desai. 1996. XKCM1: a *Xenopus* kinesin-related protein that regulates microtubule dynamics during mitotic spindle assembly. *Cell.* 84:37–47.

Wynshaw-Boris, A., and M.J. Gambello. 2001. LIS1 and dynein motor function in neuronal migration and development. *Genes Dev.* 15:639–651.

Zhang, D., G.C. Rogers, D.W. Buster, and D.J. Sharp. 2007. Three microtubule severing enzymes contribute to the "Pacman-flux" machinery that moves chromosomes. *J. Cell Biol.* 177:231–242.

Zhou, G., K.A. Mihindukulasuriya, R.A. MacCorkle-Chosnek, A. Van Hooser, M.C. Hu, B.R. Brinkley, and T.H. Tan. 2002. Protein phosphatase 4 is involved in tumor necrosis factor-alpha-induced activation of c-Jun N-terminal kinase. *J. Biol. Chem.* 277:6391–6398.